Chapter 1

Ultrafine-Grained Materials Fabrication with High Pressure Torsion and Simulation of Plastic Deformation Inhomogeneous Characteristics

Yuepeng Song, Wenke Wang, Miaomiao Chen, Jing Guo, Lingfeng Xu, Dongsheng Gao and Hyoung Seop Kim

Additional information is available at the end of the chapter

http://dx.doi.org/10.5772/intechopen.68360

Abstract

Utilization of severe plastic deformation (SPD) methods has provided a convenient approach for producing ultrafine-grained (UFG) materials exhibiting outstanding characteristics especially mechanical properties. HPT as one of the SPD methods can lead both to smaller grains and to a higher fraction of high-angle grain boundaries, which is an especially attractive procedure by researchers. In order to understand the nonlinearities relationship between the mechanical properties and the developed strain during plastic deformation, local deformation analysis using the finite element methodwas applied for the HPT process. In this chapter, results are reported of an investigation on the deformed microstructure and mechanical properties of different materials samples during the HPT process using experiments and FEM simulations. Simulation results indicate that the disks show inhomogeneity development and distribution of strain and stress during the plastic deformation. Microstructure and hardness investigation results can give a well support to verify the rules of inhomogenous plastic deformation in the early stage of the HPT disks. Furthermore, the friction and anvil geometry play important roles in the homogeneity of the deformation. After the hollow cone high pressure torsion (HC-HPT), the thermal stability of $Zr_{64.13}Cu_{15.75}Ni_{10.12}Al_{10}$ BMGs is enhanced, while the elastic modulus of BMG will be decreased.

Keywords: High Pressure Torsion (HPT), Ultrafine-Grained (UFG) Materials, Severe Plastic Deformation (SPD), Inhomogeneous Characteristics, Finite Elements Method (FEM)

1. Introduction

In recent 20 years, the investigation on the micro-structural evolution of ultrafine-grained (UFG) materials surged tremendously due to outstanding characteristics of UFG materials, especially mechanical properties [1–4]. UFG materials are defined as materials having equiaxed microstructures with average grain sizes less than 1 μm and with a high fraction of boundaries having high angles of misorientation. These UFG structures divide into materials having submicrometer materials where the grains are within the range of 0.1–1 μm and true nanometer level materials where the grain sizes are <100 nm. As described elsewhere, many literatures reveal that the UFG microstructures may additionally contain having sizes of the order of <50 nm and these observations led to the introduction of the nanometer level materials [4–12].

Severe plastic deformation (SPD) processes have been studied extensively and used as convenient methods to manufacture ultrafine-grained, nanostructured metals, and their alloys [13–15]. Recently, several processing techniques existing metal forming processes have been designed such as continuous cyclic bending (CCB), twist extrusion (TE), equal channel angular pressing (ECAP), and so on. New techniques are often proposed, all of them rely on the idea that a high hydrostatic pressure is necessary to avoid cracking, for a review see [16–25]. Among these SPD methods, the HPT process is particularly noteworthy because it can produce finer grains, with a higher fraction of high-angle grain boundaries, than can the other SPD methods [5, 8, 26–29].

The origin of HPT processing may be traced to a classic literature, written by Bridgman and published in the Journal of Applied Physics in 1943, entitled "On Torsion Combined with Compression" [30]. This fundamental concept formed the basis of a series of experiments conducted by Professor Bridgman, the Hollis Professor of Mathematics and Natural Philosophy at Harvard University.

The constrained HPT is the main study point presently, in which there was some limited outward flow of material between the upper and lower dies. The principle of the constrained HPT process is that a sample, generally in the form of a thin disk, is subjected to high pressure between massive anvils and then processed through the application of torsional straining. One die is turned at a given rotation speed and surface frictional forces deform the sample by shearing so that deformation proceeds under a quasi-hydrostatic state. The HPT process consists of two stages based on the motion of the lower dies and the samples, as shown in **Figure 1**: first the compression stage and next the torsion stage.

During the torsion stage, the compressive pressure is generally kept constant. The high-imposed compressive hydrostatic pressure prevents any cracking of the sample inside of the die, and the low thickness to diameter ratio results in the production of a high strain during the die rotation.

Although the general principles of HPT processing were first proposed over 70 years ago, the processing has become of general scientific interest only within the last 20 years.

http://dx.doi.org/10.5772/intechopen.68360

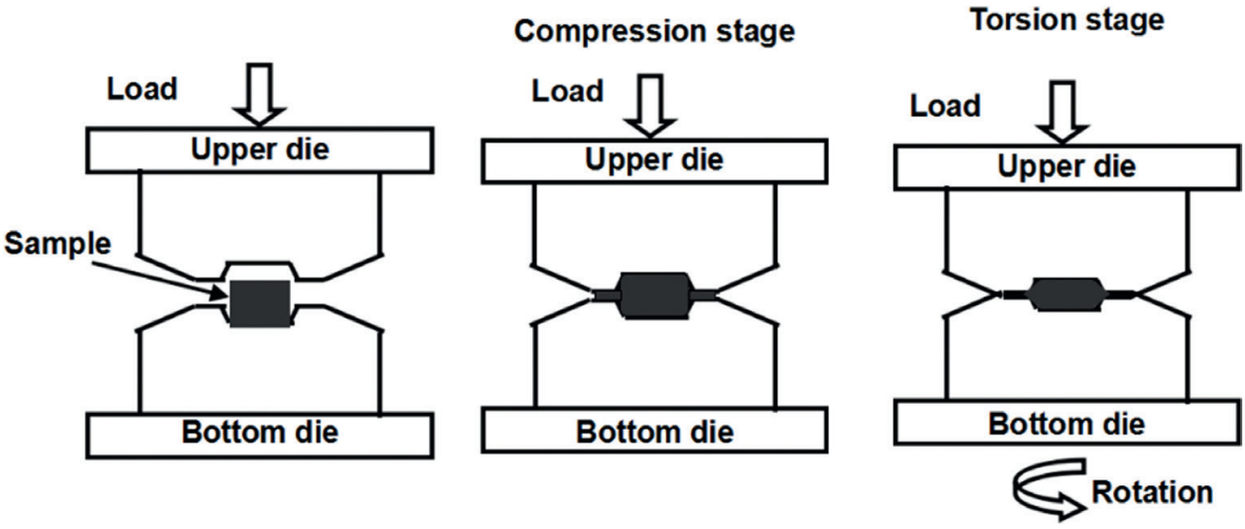

Figure 1. Schematic diagram of high-pressure torsion processing.

Moreover, it is only within the last 10 years that a number of extensive reports documenting the processing and properties of materials produced by HPT have started appearing in the scientific [5, 26, 27].

In the range of 20 years, there are many reports on preparing bulk UFG metallic materials with high pressure torsion. Kaveh Edalati form an ultra-grained structure with a grain size of ~180 nm with pure Hf by high pressure torsion under pressures of 4 and 30 GPa. In the study of I. Sabirov, Al6061-10 pct SiC and Al6061-20 pct Al_2O_3 powder metallurgy (PM) MMCs with clustered particle distribution in the as-fabricated condition are subjected to HPT at room temperature. The evolution of the microstructure during HPT is investigated. D. Gunderov from the Ufa State Aviation Technical University produced nanocrystalline $Ti_{49.4}Ni_{50.6}$ alloy in the shape of a disk 20 mm in diameter using high pressure torsion successfully. The effect of an UFG structure formed in an aluminum alloy 1570 using severe plastic deformation by HPT at room temperature and at temperature of 100 and 200? on the mechanical properties (strength and plasticity) has been investigated by M. Yu. Murashkin. Disks of $Cu_{60}Zr_{20}Ti_{20}$ composition were produced with HPT by Zs. Kovacs and the inhomogeneous microstructure of the central region consist of particles of about 50 μm and a surrounding matrix.

Presently, there are at least three aspects existing controversy in HPT field: Firstly, HPT processing consists of two stages (compression stage and torsion stage under high pressure stages, as shown in **Figure 1**). Most of the reports published focused on the last stage [32, 36–38], but there are few researchers directly on the role of compressive processing stage [39, 40]; second, because the developed strain at the center of the disk is theoretically zero and linearly increases with the distance from the center according to the characteristics of torsional strain, it is reasonable to anticipate that the microstructures produced by the HPT process will be extremely inhomogeneous. However, recently, papers demonstrated that the microstructure is reasonably homogeneous across the disks when the torsional straining continues; at last, although a lot of studies have been done on HPT [32, 36–40], most of them are for microstructure and its

characterization or for processing. Because the mechanical properties of the deformed material are directly related to the effect of friction, that is, the understanding of the effect of friction is very important in HPT.

There are many reports on radial inhomogeneity in the HPT processed metallic materials [5, 31, 32]. However, a significant dichotomy is revealed by the experimental data available. Some results gave the significant variations in the values of the microhardness and microstructure across the diameters of disks processed by HPT for austenitic steel, Cu, and high-purity Ni, given the results of lower hardness values in the centers and higher values in the peripheral regions of the disks [4, 33, 34]. On the other hand, recently, results shown that, as to commercial purity Al, an Al–Mg–Sc alloy, Cu and high-purity Ni materials, when torsional straining is continued to a sufficiently high total strain, the microstructures and hardness become reasonably homogeneous across the disks [5, 34]. Considering this case, the jobs of hardness and microstructure inhomogenous distribution inspection are very important to explore the deformation mechanism during the HPT process.

Because the mechanical properties of the deformed material are directly related to the amount of plastic deformation, that is, the developed strain, understanding the phenomenon associated with strain development is very important in severe plastic deformation process. Meanwhile, in the recently three decade, computer simulation and finite elements method (FEM) have been attracted with huge interests by more and more researchers of widely fields, and they can be used to explore and gain new insights and formation mechanism study in materials preparation process.

In this chapter, results are reported of an investigation on the plastic deformation inhomogeneous characteristics of different materials samples during the HPT process using experiments and FEM simulations.

2. Experimental conditions and simulation procedures

2.1. Materials and samples

In the previous works, there are two materials disks processed by HPT: One is commercial purity copper (99.98 mass%), and the other is IF steel manufactured by the Pohang Steel Company (POSCO, Korea) with the composition of 0.0026 wt% C, 0.096 wt% Mn, 0.045 wt% Al, and 0.041 wt% Ti. The state of the two materials is listed in **Table 1**. In addition, hollow cone $Zr_{64.13}Cu_{15.75}Ni_{10.12}Al_{10}$ bulk metallic glass (BMG) was prepared by sucking into a copper mold.

For the HPT experiments, materials of copper and IF steel with six magnitudes of pressure of 1, 2, 4, 6, 8 and 10 GPa were imposed on the disks at room temperature. The applied revolutions of the bottom die are 0, 1/4, 2/4, 3/4, and 1 turns under the provided pressures. The time of applying the compression loads was set as 10 s, and the strain rate in the disk was low enough to ignore any thermal effect.

Finally, in the HPT experiments of $Zr_{64.13}Cu_{15.75}Ni_{10.12}Al_{10}$ alloy, the ingots were produced through alloying high-purity elements (minimum 99.9 wt%) in an arc furnace under an

Initial state	Copper	IF steel
Original state	Cold-drawn state	plate 12 mm in thickness size rolled from casting ingot
Homogenizing heat-treatment	600°C × 2 h, cooling in furnace	700°C × 2 h, cooling in furnace
Sizes of HPT disks	9.5 mm in diameter and 2 mm in thickness	19.5 mm in diameter and 2 mm in thickness
Grains size	20–40 μm	150–200 μm
Original hardness	~56 Hv	~80 Hv

Table 1. State of the two materials disks.

argon atmosphere. The remelted alloy ingots were suction cast into a Cu mold in order to obtain hollow cone specimens with base diameter, cone height, and wall thickness were 19.8, 14.0, and 1.2 mm, respectively. A hollow cone specimen of Zr-based BMGs is set on the concave die; then, a convex punch is inserted into the specimen; last, the preset pressure (40 tons) and rotation angle (1 reverse turn) are applied to the hollow conical specimen, as shown in **Figure 2**. The primary difference compare with the above HPT process is the sample shape, which is a hollow cone in the HC-HPT process rather than a disk in the HPT process.

2.2. Measurement devices and approaches

For the measurement of copper and IF steel, there are two inspection planes along with different direction of disks: One is radial plane (following the longitudinal direction of disks), and the other is transversal plane (following the transversal direction of disks). On transversal plane, the hardness of points on different diametrical direction is measured, whose angle between the adjacent direction is 30°. The distance between the adjacent testing points is 0.25 mm for 9.5 mm diameter and 0.5 mm for 19.5 mm diameter. As to the radial plane, the distance between the adjacent testing points is 0.1–0.3 mm at axial direction and 0.5 mm at radius direction. The schematic drawing of sampling positions and the measurement of hardness distribution of different positions are shown in **Figure 3**.

Hardness was measured using FM-700 Microhardness Tester, and the pressure loading is 100 g, continuous 10 s. All of hardness data are processed by Origin software. The color-coded contour maps and curves of hardness distribution of different samples are so obtained. Microstructures in different position of disks were observed using optical microscopy (Olympus U-TV0.5xc) and electron backscattered diffraction (EBSD).

The microstructure of $Zr_{64.13}Cu_{15.75}Ni_{10.12}Al_{10}$ alloy was determined using D/max-rB X-ray diffractometer with Cu Kα radiation, and the wavelength of the X-rays was 0.154 nm. Differential scanning calorimetry (DSC 404, Netzsch, Germany) was performed at a constant heating rate of 0.667 K/sec under a constant flow of argon. The dilatation measurements were executed using a conventional dilatometer (DIL 402C, Netzsch, Germany).

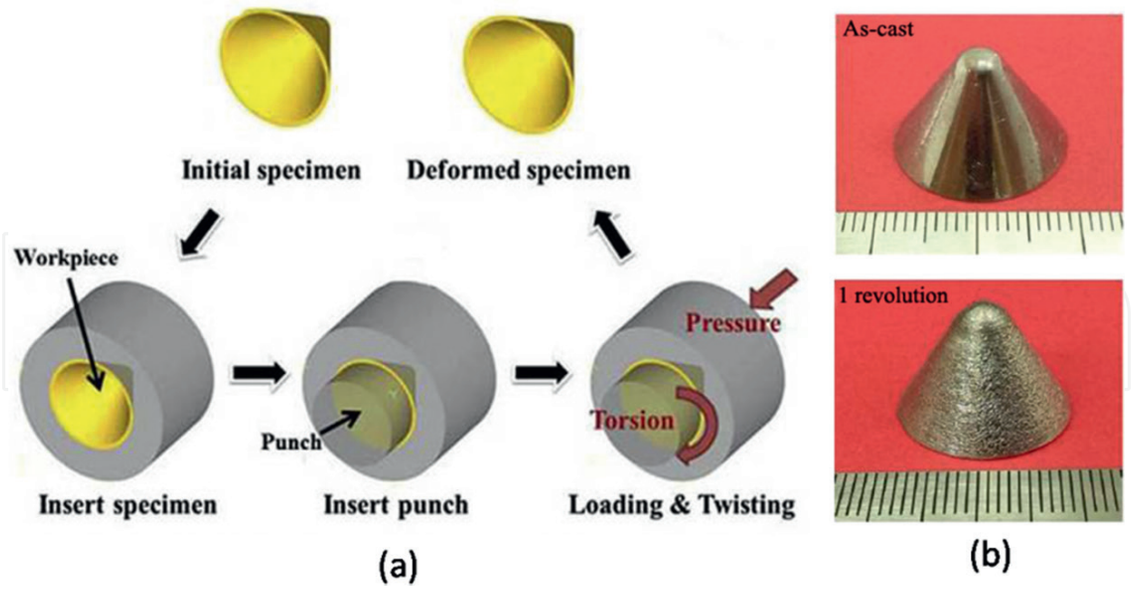

Figure 2. (a) Schematic diagram of HC-HPT procedure and (b) samples.

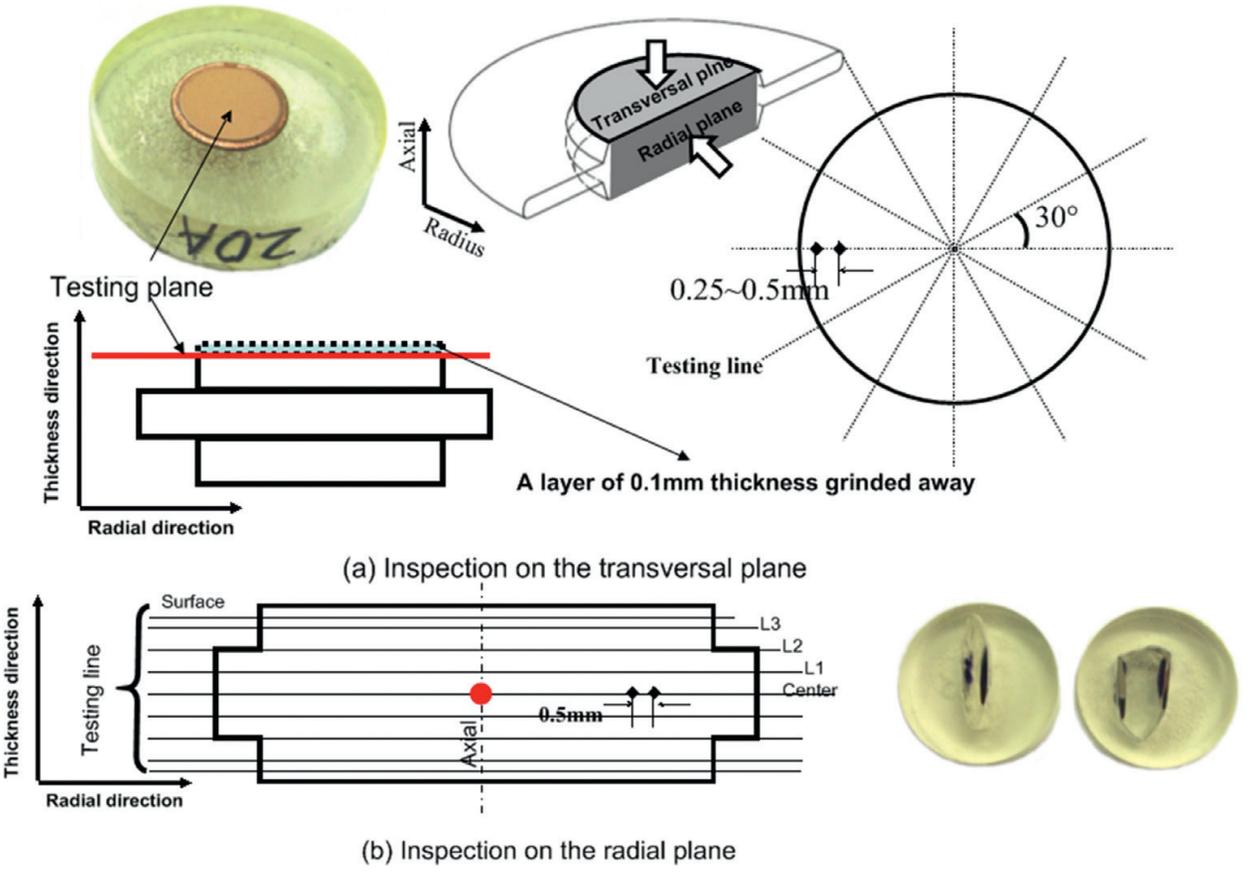

Figure 3. Schematic drawing and the measurement of hardness distribution of disks.

2.3. Simulation conditions and procedures

Plastic deformation behavior, hardness, and microstructure distribution of HPT processed disks are investigated using experimental approach and simulation approach with the finite element method (FEM). With ANSYS10.0 program simulations, the deformed microstructures and mechanical properties of copper disks in the compressive stage of HPT processing are investigated. Meanwhile, a commercial rigid-plastic finite element code (DEFORM 3D; Scientific Forming Technologies Corporation, USA) was used to simulate and understand the local plastic deformation of the IF steel disks in the torsion stage of the HPT process.

2.3.1. Simulation procedure of copper disks in the compressive stage of HPT with ANSYS

The simulation of die material is alloy steel, and the properties data come from the web site [41] and testing experiment. The simulation procedures of the copper at the compression stage of HPT are as follows:

Step 1: Build geometry. The sizes of the sample in ANSYS correspond to the experimental disk.

Step 2: Define material properties. The Young's modulus and Poisson's ratio of materials are 110 GPa, 0.343 for copper and 220 GPa, 0.32 for alloy steel, respectively [41]. The fiction coefficient between disk and anvil is 0.06.

Step 3: Define element types. For the analysis of the copper deformation, Plane 182, Target 169, and Contact 170 are selected to define the sample, the surface of the target and the surface of the contact, respectively.

Step 4: Generate mesh and create contact pair. There are about 40,000 elements meshed in the copper disks model. The meshed model is shown in **Figure 4**.

Creating contact pair using Contact Wizard with the two element types: Target 169 and Contact 170 are very important for this contact analysis.

Step 5: Apply loads. For this simulation, it needs to apply symmetry constrains on the axis of the copper sample, because the device of HPT is axis symmetrical shape.

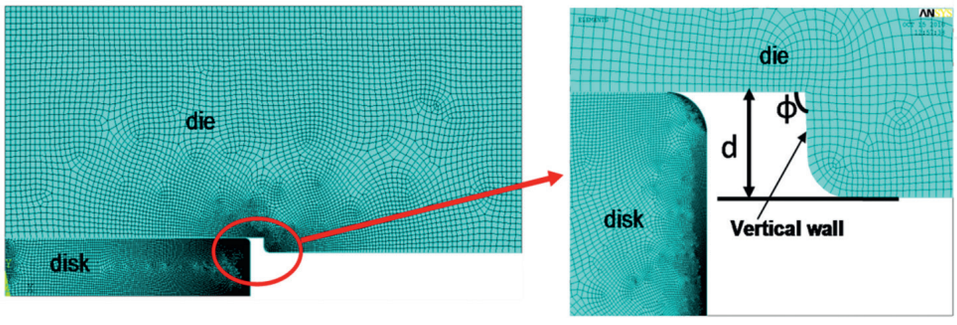

Figure 4. The meshed simulation model.

Step 6: Obtain solution and review results. Some results can be got from the general post-processor, such as the stress and the strain distribution of the compression sample, and the deformed shape.

2.3.2. Simulation procedure of IF disks of HPT with DEFORM

A local deformation analysis using the FEM should be carried out in order to better understand HPT processing and the material's response to the dies in HPT. In this work, isothermal FEM simulations of the HPT process were carried out using the commercial rigid-plastic finite element code.

In the FEM simulations, the initial dimensions of the disks were 20 mm diameter and 2.0 mm thickness. In the compression stage, the speed of the top anvil was 0.1 rad/s up to a full turn. The friction between the die and the sample was set to satisfy the sticking condition, as the roughness of the die surface was high enough to prevent slippage between the sample and the die. We used the materials parameters for the simulation from the database of DEFORM code-0.08% C carbon steel, and the Poisson's ratio of material is 0.3. HPT dies: rigid body. The number of the initial mesh in the sample was 25521, and this number of elements was enough to show the local deformation of the sample by calculation without changing the number of elements. The times of the compression stage and torsion stage were all set at 10 s.

3. Properties and microstructure inhomogeneity of different materials disks processed by high-pressure torsion

3.1. Inhomogeneous distribution of mechanical properties and microstructure in the compression stage of HPT

Since plasticity is path dependent, unlike elastic deformation, the deformation that occurs at both stage I (compression) and stage II (compression + torsion) is important for the properties and microstructures of HPT processed materials. Although many reports have been published recently on the microstructural evolution, hardness distribution in HPT processed samples, and torsional behavior [4, 7–12], all of them ignores the stage I deformation, and no studies on the properties of samples after the compression stage have been done, as far as can be determined. For example, Edalati et al. [42] investigated the microstructures and mechanical properties of pure Cu processed by HPT and proposed a unique single curve of hardness against the equivalent strain; however, they did not consider the stage I deformation and the compressive component of strains in their equivalent strain. Nowadays, more and more results indicated that the stage I deformation influences the stage II deformation [43]. Hence, explaining the HPT behavior without considering the stage I deformation is not sufficient for full understanding.

In this section, the commercial purity Copper (99.98 mass%) and IF steel are used as the study materials. For the experiment of copper, two applied pressures of 2 and 8 GPa were imposed at room temperature on the disks with the velocity range of 1/2 rpm and the time of compression

http://dx.doi.org/10.5772/intechopen.68360

load of 10 s. For the IF steel during the compression stage of HPT, the applied pressures were imposed at room temperature on the disks for 0.6, 1.25, 1.9, and 2.5 GPa, respectively.

Figure 5 shows the hardness distribution of copper disks with 2 GPa pressure given the color-coded contour maps and distribution curves. As shown, L1, L2, and L3 are the testing lines position at the distance of 0.25, 0.5, and 0.65 mm from central plane of disks' thickness direction, respectively. The hardness shows almost symmetrical distribution on the thickness direction from upper to bottom surface of compressed disks (**Figure 5a**).

Furthermore, it also indicates an inhomogeneity distribution, giving lower hardness in axial center near the surface, higher hardness in edge and the uniform hardness in radial medium, which is also clearly displayed in **Figure 5b** (L2, L3). However, a higher hardness zone exists in axial center near the central plane. Compared with the hardness of 56 Hv in the initial state, the hardness of disks remarkably increases at the compressive stage of HPT, which is different in the different position, that is, the hardness on the central plane is 106.9, 101.2, and 112.3 Hv in the center, radial medium and edge, respectively. Further investigation indicates that the hardness distribution of compressed disk with 8 GPa has a similar trend with the former results (**Figure 6**).

It is well known that the mechanical properties are mainly dependent on the microstructure condition. The detailed investigations are focused on the relationship between the microstructure and the mechanical properties, as shown in **Figure 6**. Clearly, there is a remarkable inhomogeneity distribution on the testing plane, for not only hardness but also microstructure.

In the edge zone, there is a thin layer with grains hardly change as the same as the initial state; however, a little more inward, the grains proceed large severe plastic deformation, and their boundaries become very obscure. In the center zone, some grains occur plastic deformation but others have no any change. And the grains have a uniform deformation in the radial medium zone of compressed disks. Based on the Hall-Petch relationship, the inhomogeneity distribution of microstructure can support the ones of hardness, giving lower hardness in

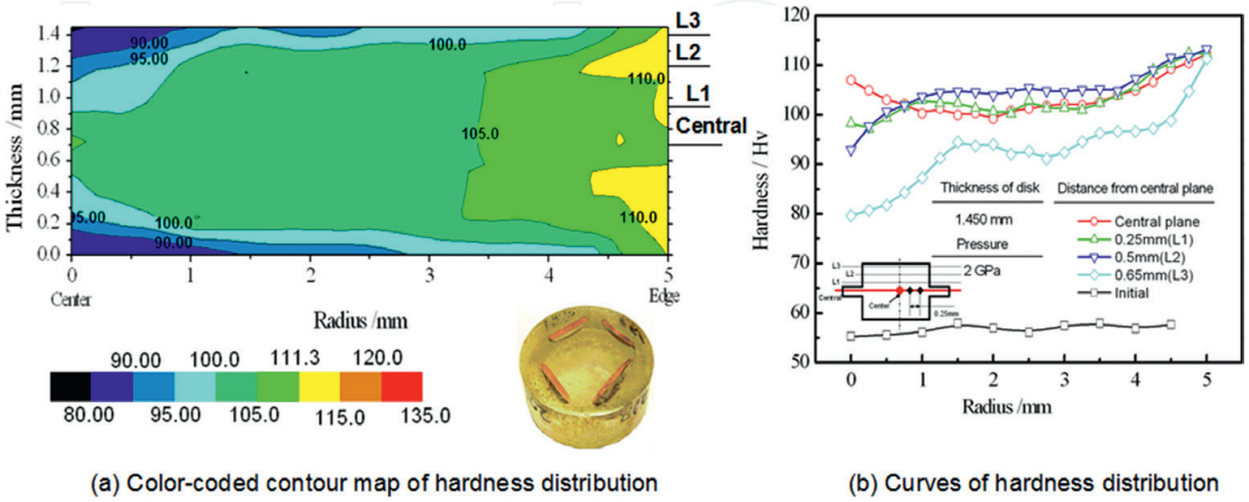

Figure 5. Hardness distribution of compressed disk with 2-GPa pressure.

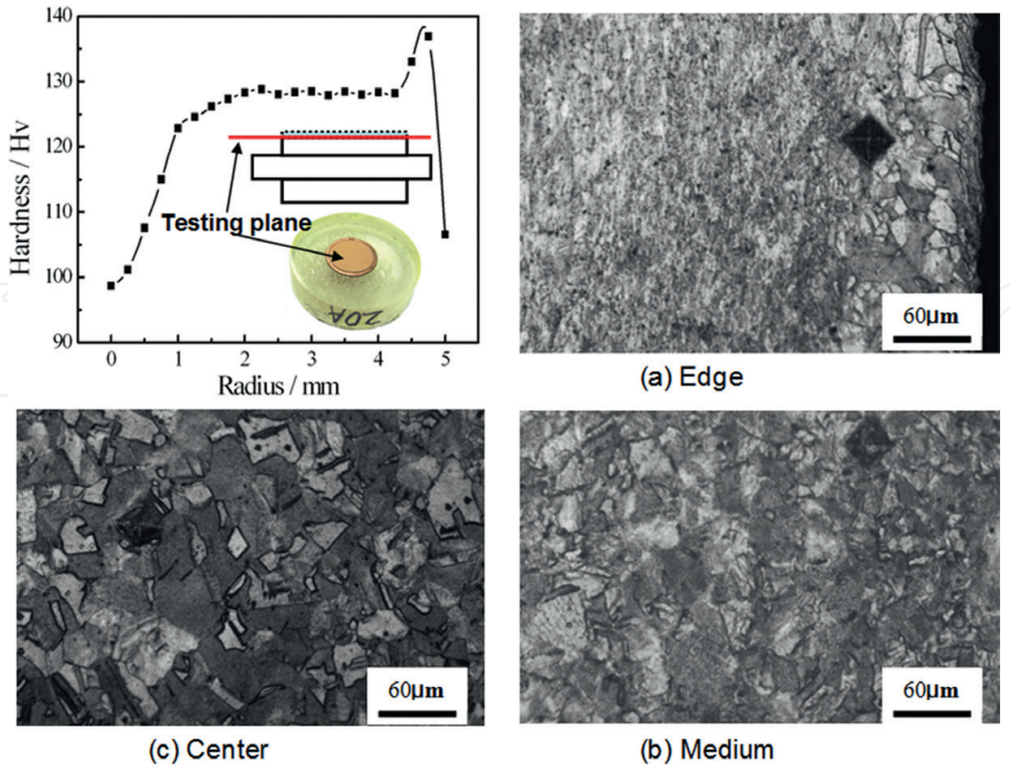

Figure 6. Hardness and microstructure distribution of compressed disk with 8-GPa pressure.

center, uniform hardness in medium, and higher hardness in edge. Of course, there is a little soft layer in the outer edge of the compressed disks.

As the former mentioned, the inhomogeneity of hardness and microstructure distribution in the compressive copper disks of HPT really existed. Of particular concern is that, as to IF steel disks, whether this inhomogeneity also existed at the compression stage during HPT. The study proceeded to investigate the inhomogeneity of hardness and microstructure on the different direction of HPT processed IF steel disks at the compressive stage.

Figure 7 displayed the hardness distribution on the transversal plane (0.1 mm distance from the surface) and the hardness variation of different position along with the compression. As the almost same distribution with the copper disks given by literature and formerly research, at the compressive stage of HPT, the hardness distribution of IF steel disks is also inhomogeneous, given high value in edge, considerable uniform in medium and low hardness in center [5, 35].

On the radial testing plane, the hardness distribution is also inhomogeneous, and the color-coded contour maps are shown in **Figure 8**. As shown, the hardness is almost symmetrical distribution from upper to bottom surface of disks for the central of thickness as the symmetry plane, which is also reported by Pippan [44]. The hardness distribution on radial testing plane is the same with that on the transversal testing plane formerly obtained, which presents high hardness in edge, uniform hardness in medium, and low value in center.

http://dx.doi.org/10.5772/intechopen.68360

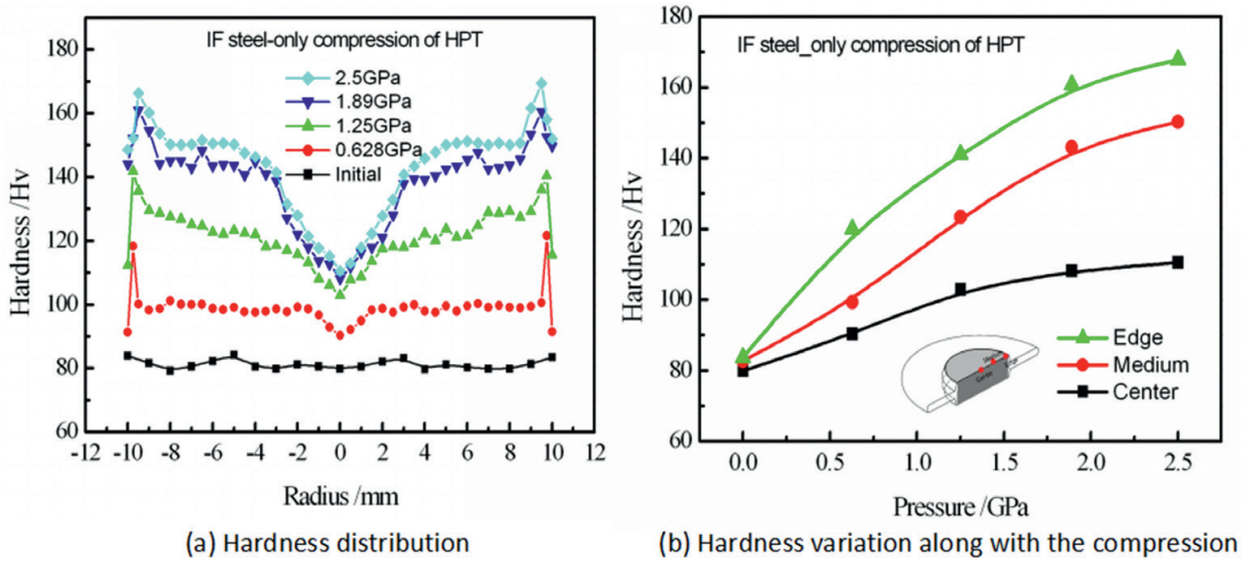

Figure 7. The hardness distribution on the transversal testing plane of different samples at the compressive stage of HPT.

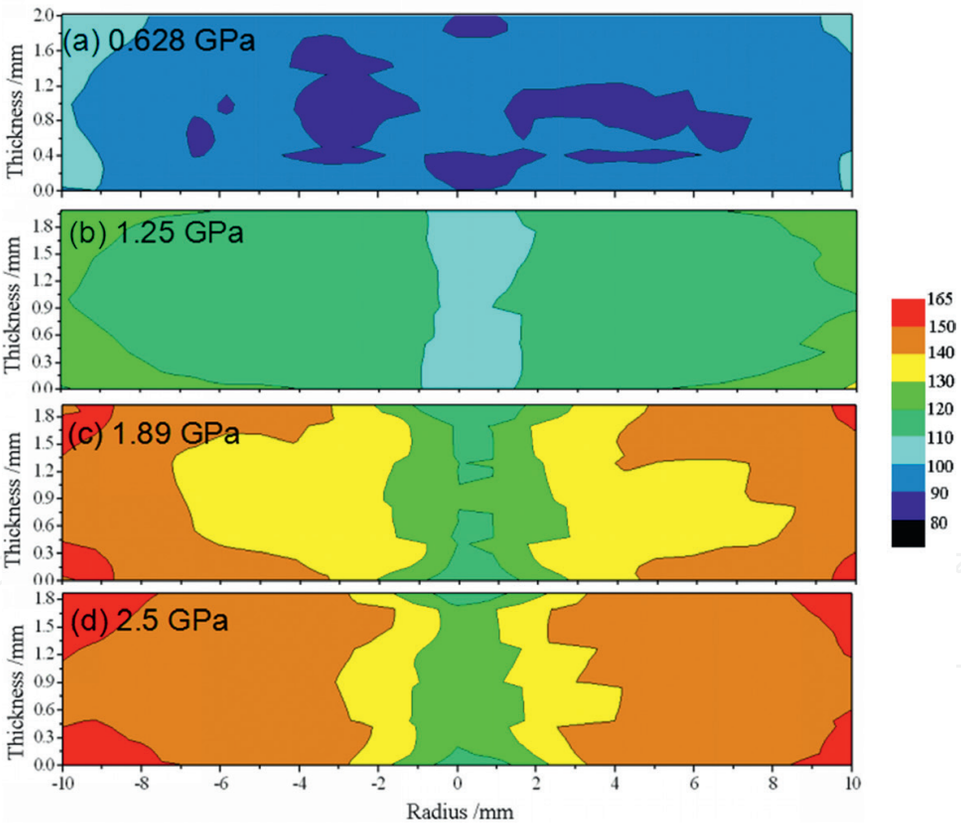

Figure 8. Color-coded contour maps of hardness distribution on the radial testing plane of compressed IF steel disks.

In addition, there exists a soften region near the surface, and higher pressure is, less area is. An important point should be paid attention to that the lower hardness areas are only in both the outedge and center near the disks' surface. However, a high value of hardness exists near the central position on the thickness direction named hardness hill from literatures [35, 36].

In order to clearly display this inhomogeneity, the edge microstructure on the different testing plane (transversal and radial) of compressed disk under 2.5 GPa pressure is shown in **Figure 9**. The same position on the two testing planes is corresponding with each other. For this disk, in the outer boundary, there exists a soften region resulting to the lower hardness (as the arrow direction). The severe deformation grains on the transversal plane are corresponding with the flow lines clearly displayed on the radial plane.

Another fact need to be paid attention is that as to the flow-line, the angle of direction between its texture and pressure is about 45°, which is the most flexible deformation direction under the shear slip for grains. Further microstructure inspection results show that the grains near the surface display more and more remarkable texture characteristic microstructure from center to edge along with the radius direction of the compressive disks.

However, the grains of the thickness central position haven't this characteristic texture microstructure. The close-up microstructure view from edge to center of compressed disks of 2.5 GPa pressure is listed in **Figure 10**. The results can also strongly support the former conclusion.

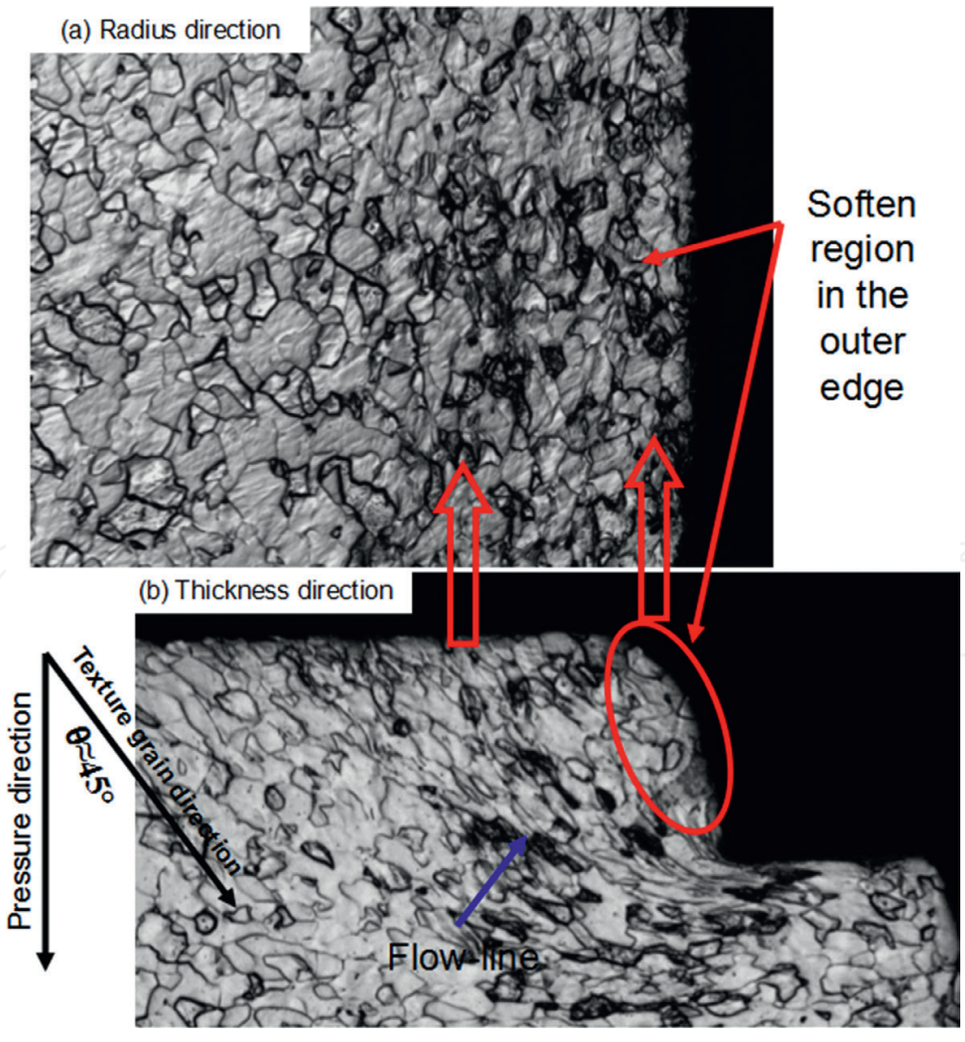

Figure 9. Edge microstructure on the different testing plane.

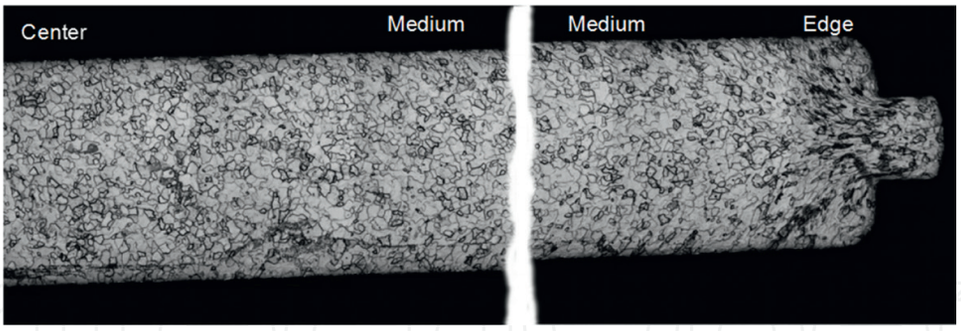

Figure 10. Close-up microstructure view from edge to center of compressed disks.

3.2. Mechanical properties and microstructure at the torsion stage of HPT

The principles of the modern HPT process have already been described extensively in the literature [5, 45, 46]. In brief, the initial coarse-grained solid or powder sample for HPT is located between two hard anvils, where it is subjected to a compressive applied pressure (P) of several GPa at room temperature (or a warm temperature), and then, a torsional strain is imposed by the rotation of the anvil. The surface frictional force generates the deformation of the disk through the torsional shear, thereby a large deformation proceeds under a quasi-hydrostatic pressure. In practice, the effective strain imposed on the sample may be defined as follows: $\varepsilon_{eq} = 2\pi NR/\sqrt{3}h$ where N is number of turns in the HPT, R is the distance from the center of the sample, and h is the sample thickness [5, 47, 48]. From the formula, following the radius direction from center to edge of HPT disks, along the R increasing, the equivalent von Mises strain is higher to higher which means the deformation of material more and more severe.

In this section, the development of deformed microstructures and mechanical properties of the IF steel disks are presented at the early torsion stage of the HPT process using experiments approaches. The applied pressure and degree of revolutions during the torsion stage were 2.5 GPa and 0, 1/4, 2/4, 3/4, and 1 turns, respectively. **Figure 11** presents the hardness distributions on the radial-axial plane of the HPT processed IF steel disks.

Exhibiting the same trend as in the literature, the Figure clearly indicates lower hardness values in the center and higher values at the edges: after 1 turn, the hardness values in the center, middle, and edge were 140, 160, and 375 HV, respectively. Compared with the disks after torsion, in the center, the soft region penetrates through the upper and bottom surfaces of the compression-only disk (0 turns), and it disappeared after 1 turn. Furthermore, the soft region shrunk as the degree of revolutions increased. The large deformation and high hardness (240 HV) proceeded at a distance of 6 mm from the center of the disks (1/4 turn) and at a distance of 4 mm from the center of the disks (1 turn). That is, a severe deformation will proceed gradually from the edge to center along with increases in the degree of revolutions at the early torsion stage of the HPT process.

A layer that is 0.2 mm from the surface of the HPT-processed disks was ground and polished. The hardness on the testing plane along the radial direction is shown in **Figure 12**.

Figure 13 shows the hardness on the testing plane along the radial direction. As shown, the hardness trend on the transversal direction at the early torsion stage in the HPT process is

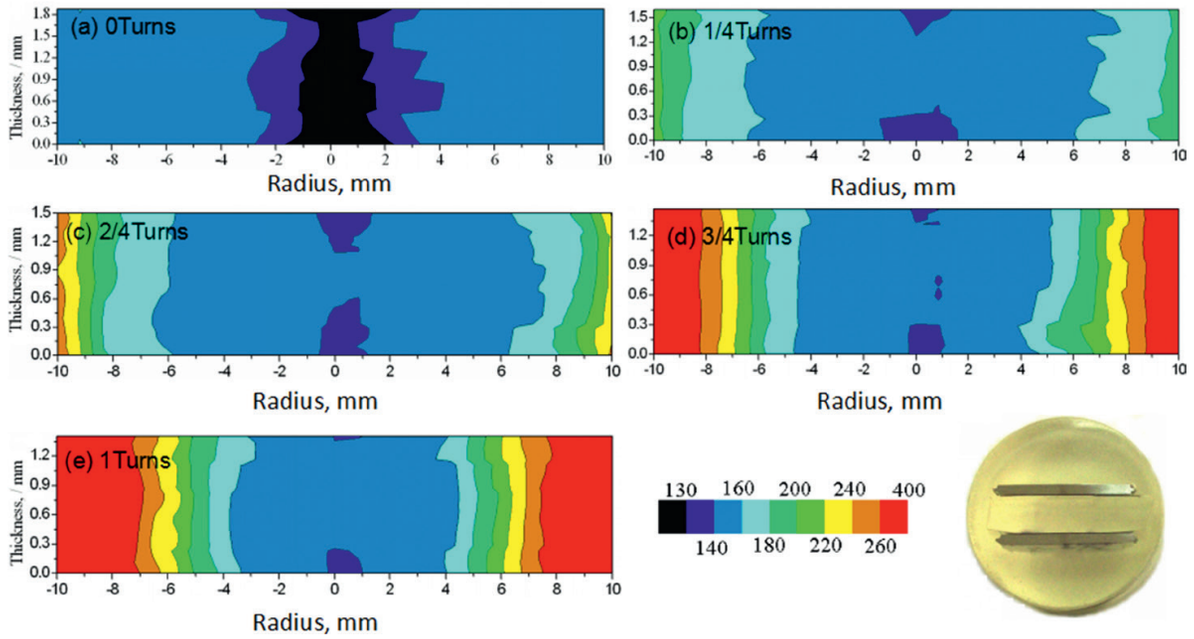

Figure 11. Hardness distribution on the radial-axial plane.

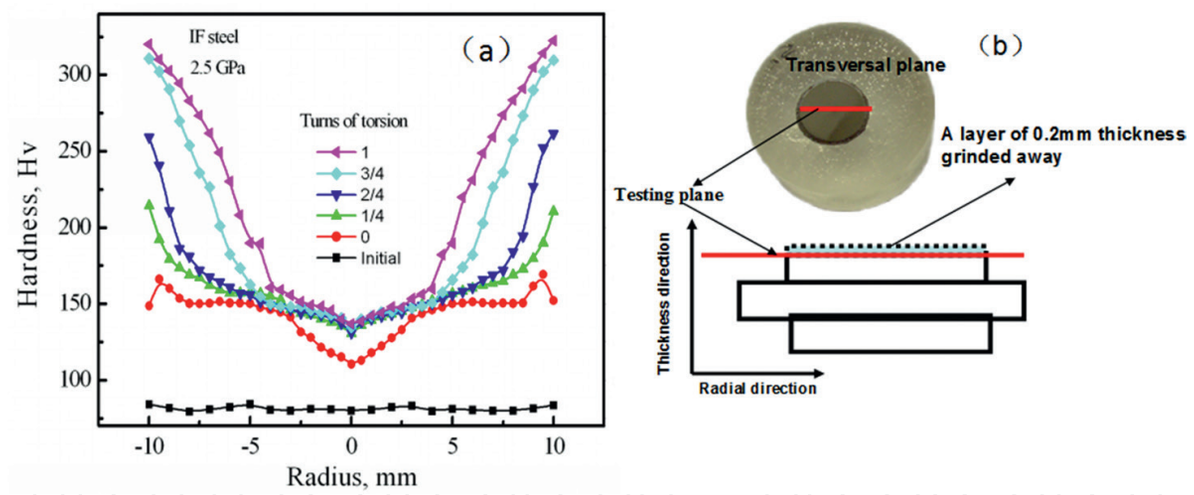

Figure 12. Hardness variations from the center to the edge (a) and the measuring plane (b).

the same as those along the radial direction. Similar to the compression stage, the different mechanical properties at the torsion stage could be explained by the microstructure state, as shown in **Figure 14**. Without torsional straining (0 turns), the grain boundaries are clearly observed, and the grains are insufficiently equiaxed. In contrast, after an additional revolution in the same torsional direction to give 1 turn, the grain boundaries become obscure, and the grains are reasonably equiaxed.

The images in **Figure 14e** show inverse pole figures (IPF) with the boundary map having the information on the orientations of microstructure and the boundaries rotation angle. The

http://dx.doi.org/10.5772/intechopen.68360

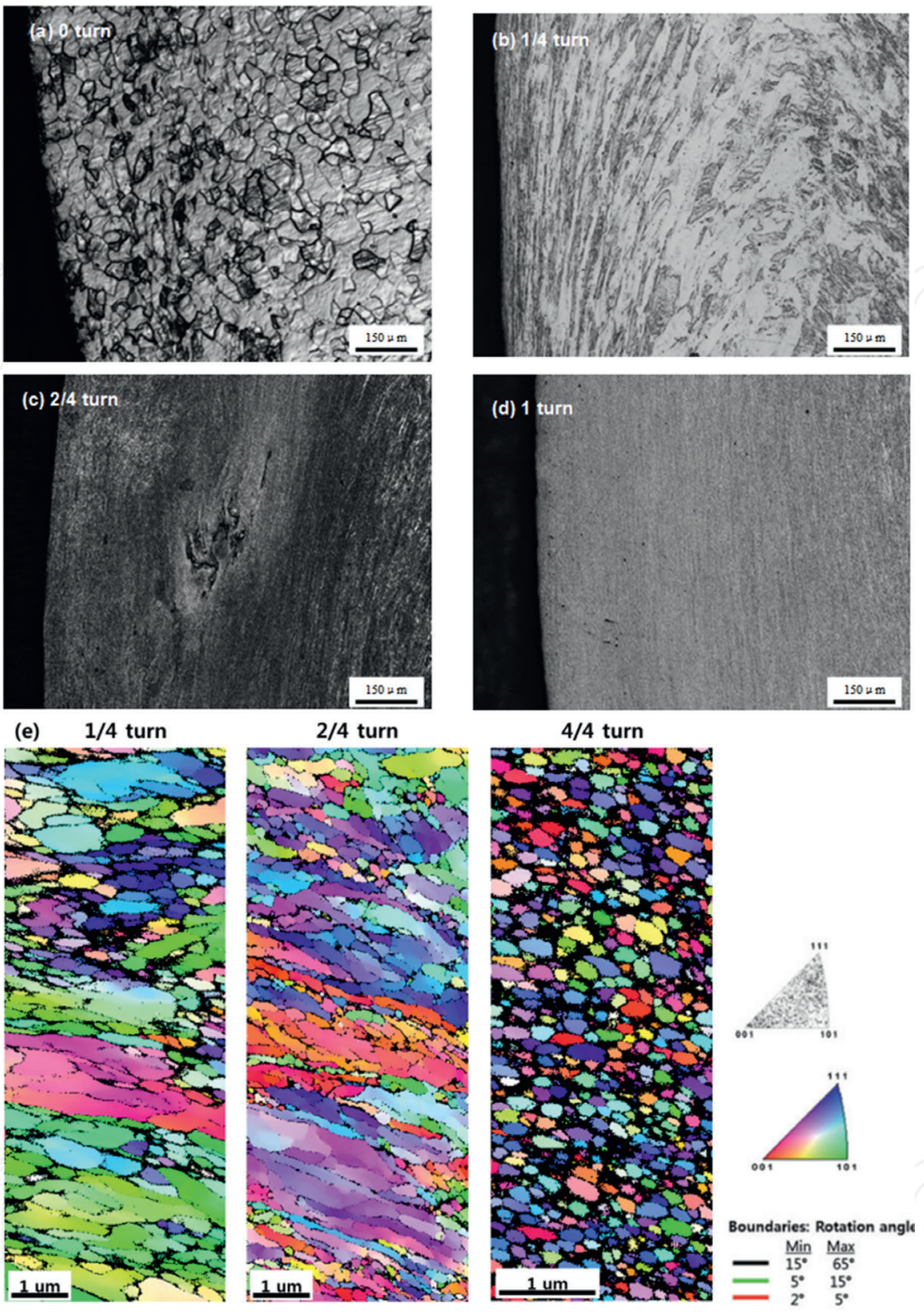

Figure 13. Microstructure at the edges of 0, 1/4, 2/4, and 1 turn HPT-processed disks using optical microscopy (a–d) and EBSD (e).

boundary map indicated high-angle grain boundaries (HAGBs: 15° <, black line) and low-angle grain boundaries (LAGBs: 2–5°, red line; 5–15°, green line). According to the EBSD results, the average grain sizes for 1/4, 2/4, and4/4 turns are 2516, 1940, and 0.308 lm, respectively. The average grain size decreases with increasing the rotation angle. After 1/4 turn, a lot of LAGBs were generated in the large grains and formed subgrains. Numerous LAGBs (green

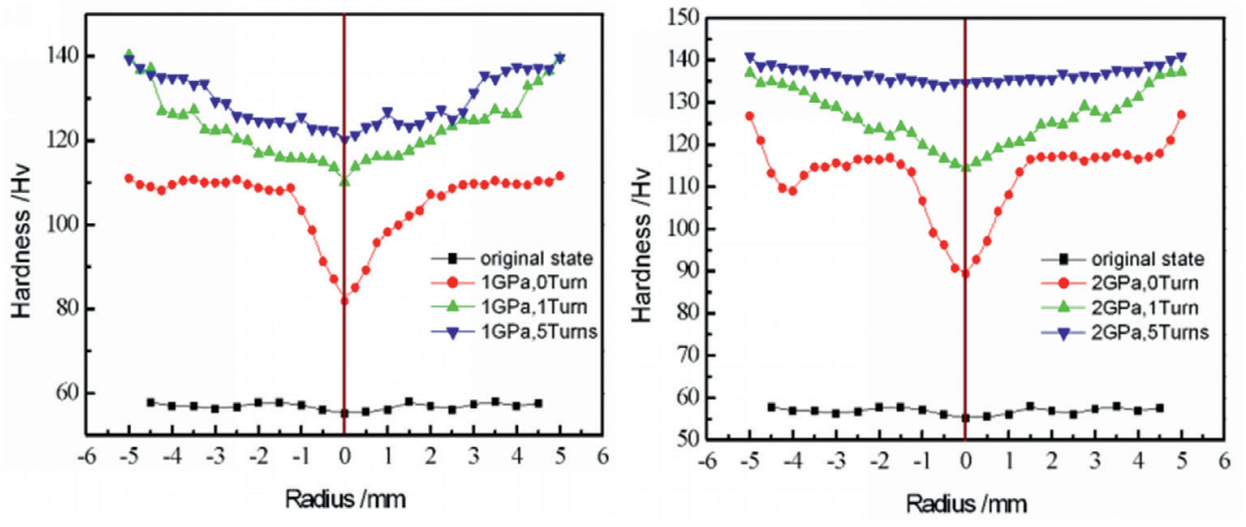

Figure 14. Hardness distribution on RP1 testing plane of different disks.

and red lines) were found within large grains, and the colors of the grains in the IPF map slightly change in the large grains. Moreover, on the top part of the image, the HAGBs are formed, and the grains are refined by recrystallization. From 2/4 turns, the fractions of HAGBs and equiaxed refined grains increased, and fine grains were located between the large grains with slightly different orientations. Finally, the average grain size with 0.308 lm was achieved after 4/4 turn with random orientation.

In the compression and the early torsion stage of HPT, the materials exist serious inhomogeneity not only in the microstructure but also in the mechanical properties. However, this is unfavorable to accommodate the following plastic strain and then highly limit the applications of HPT. Whether this inhomogeneity can be improved in the following deformation stage is a key factor for industrialized applications.

Hardness distributions on the surface plane form center to edge in 0, 1, and 5 turns HPT processed copper disks under different applied pressure are shown in **Figure 14**. The Figure clearly indicates that the hardness on the surface plane increases with increasing the degree of revolutions. However, the hardness in the center and middle zone of the HPT-processed disks varies sharply with increasing the degree of revolutions in comparison with that in the edge zone: the hardness distribution is homogeneous after several revolutions, particularly under the applied pressure of 2 GPa. That is to say, compared with the torsion stage, the hardness on the surface of the disks exhibits more inhomogeneity along the radial direction in the compression stage.

Moreover, **Figure 14** also presents that torsion can result in not only increased hardness but also uniform hardness distribution. Along the radial direction, the more the degree of revolution is, the more homogeneous the hardness distribution on the RP1 plane will be. That is, the hardness distribution becomes homogeneous with increasing the degree of revolutions.

The severe plastic deformation of copper, IF steel disks of HPT through hardness, and microstructure distribution on the testing plane of the different direction is presented. There exists

serious hardness inhomogeneity on the HPT-processed disks at the compression and the early torsion stage, showing higher hardness in edge, lower hardness in center, and considerably uniform hardness in radial medium of disks. However, according to the experiment of copper at torsion stage, the above inhomogeneity in mechanical properties is hopeful to be improved by the subsequent severe torsion deformation.

4. Experimental and finite element analysis of plastic deformation inhomogeneous characteristics of HPT disks

As is known, the mechanical properties of the deformed material are related to the amount of plastic deformation, that is, the developed strain and stress during the HPT processing. The hardness and microstructure distribution associated with the strain and stress development is very important in SPD process. Thus, for systematic analysis of deformation behavior of materials, a numerical approach is useful.

In this section, plastic deformation behavior, hardness, and microstructure distribution of HPT processed disks are investigated using experimental approach and simulation approach with the finite element method (FEM). With ANSYS10.0 program simulations, the deformed microstructures and mechanical properties of copper disks in the compressive stage of HPT processing are investigated. Meanwhile, DEFORM 3D was used to simulate and understand the local plastic deformation of the IF steel disks in the torsion stage of the HPT process.

4.1. Deforming simulation results and verifications in the HPT process

The mechanical properties of the deformed material are attribution to the amount of plastic deformation, that is, the development and distribution of strain and stress of disks during the compressive processing [49, 50]. The key factors of inhomogeneity distribution of hardness and microstructure are attributed to the inhomogeneity deformation of copper disks. That is to say, the inhomogeneous distribution of strain and stress leads to microstructure inhomogeneity. As an example of disks with 8-GPa pressure, the strain distribution simulation and the microstructure of different position are shown in **Figure 15**.

The simulation results show that there indeed exists the inhomogenous distribution of strain and stress of compressed disks. In the outer edge region, lower strain leads the grains to hardly deformation as the arrow directing in **Figures 15a** and **16a**, which corresponds to the lower hardness. Because of huge friction between disk and the vertical wall of anvil, the deformation is restrained, and this lower strain zone proceeds. However, a little more inward, severe plastic deformation occurs, and larger strain is clearly displayed in **Figure 15a** with particular flow-line microstructure, similar with the results in **Figure 9**. Moreover, the angle 45° between the slip lines and the pressure direction can be shown in the strain distribution simulation.

In the center of disks, near the surface, there is a low strain zone, and the microstructure shows that some grains deformed but others have no change (**Figure 15c**). These results can explain

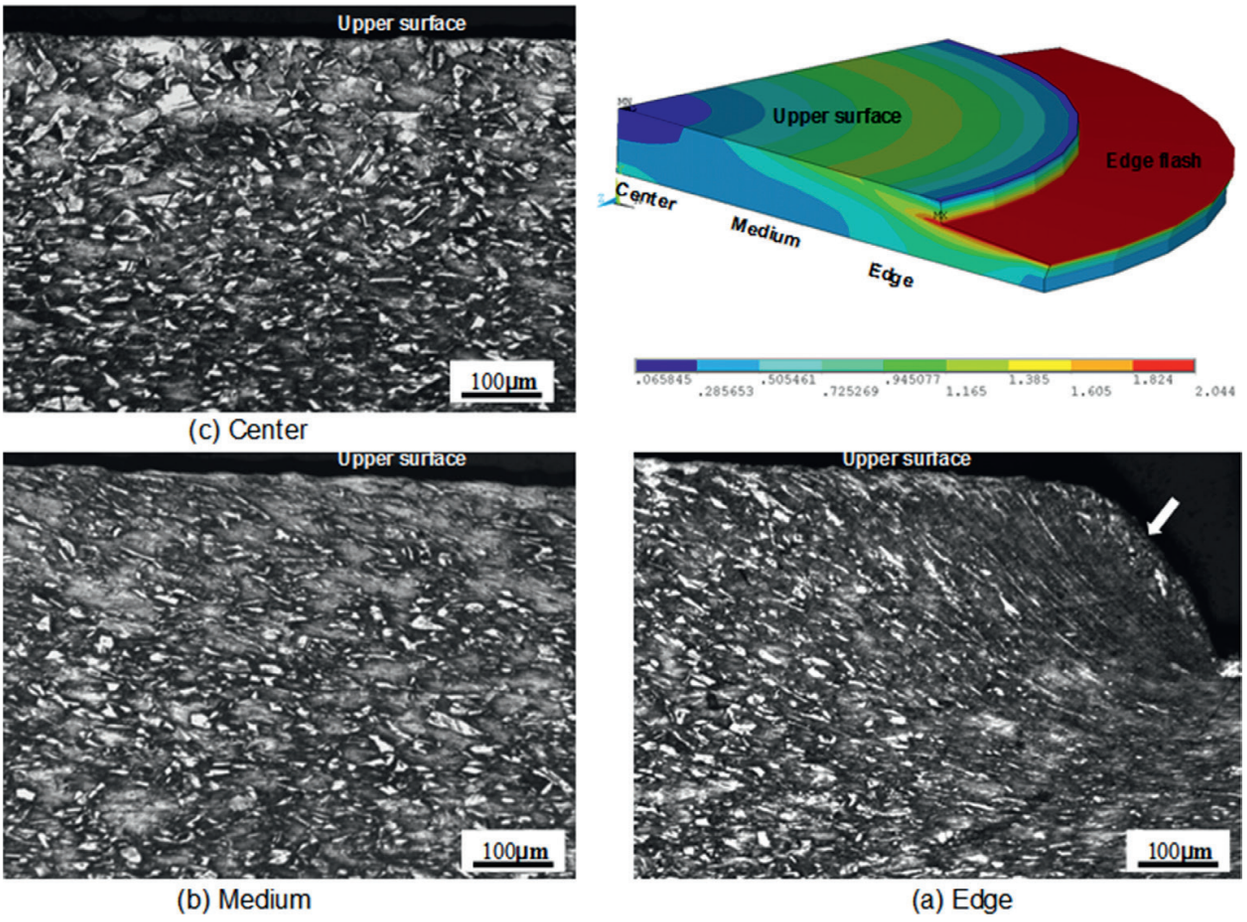

Figure 15. Strain distribution simulation and microstructure in different position of disk with 8 GPa pressure.

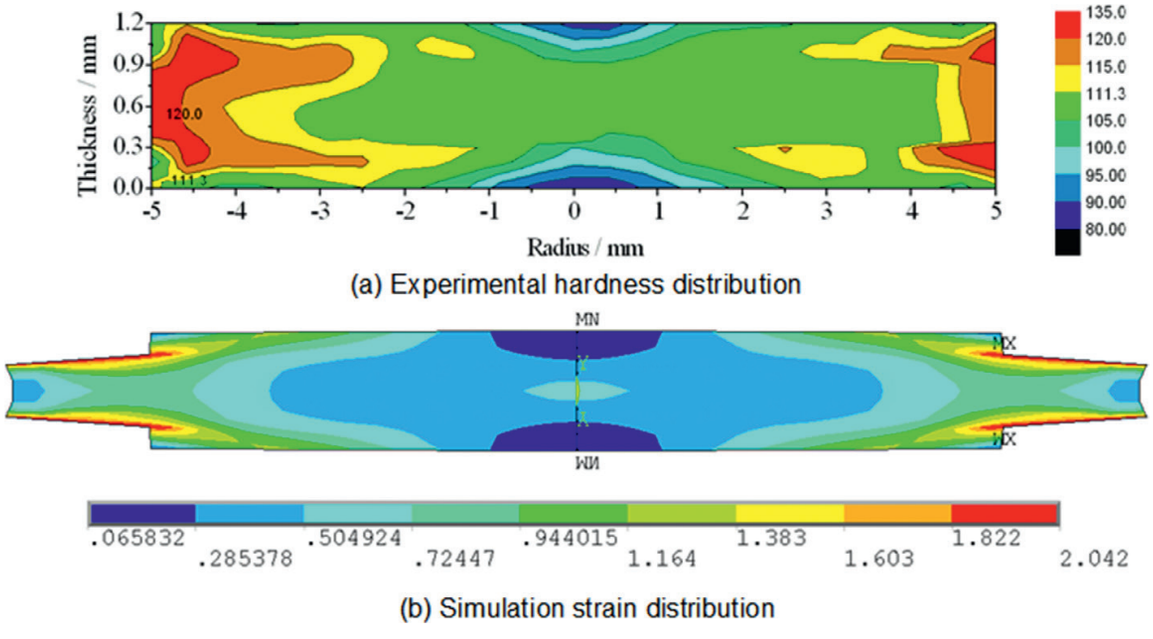

Figure 16. Hardness and strain simulation distribution of disk with 8 GPa pressure.

the reasons of the lower hardness existing in this region shown in **Figure 5**. On the other hand, near the central plane of thickness direction of disks, the strain remarkably increased with the consequence of grains deformation and high hardness.

Figure 16a is the experimental hardness distribution of disk in the axial direction and the simulation results of strain distribution of compressive disk with 8-GPa pressure.

As shown, simulation results can also verify the rules of hardness distribution on the compressive disk plane. For example, the higher hardness zone in the edge relates to its severe plastic deformation causing ultrafine grains. On the other hand, in the center, low deformation near the surface leads to low hardness corresponding with its hardly unchanged grains of the microstructure characteristic.

Subsequently, DEFORM 3D was used to simulate and understand the local plastic deformation of the IF steel disks in the torsion stage of the HPT process. In the simulation, the applied revolutions of the bottom die are 0, 1/4, 2/4, 3/4 and 1 turns under the provided pressures of 2.5 GPa, which the rotation rate of 1.256 rpm, and the coefficient of friction between the dies and the sample was assumed to be 0.12.

Figure 17 shows the integrated results including the relationships between the revolutions and hardness, the effective strain in different positions of the HPT-processed disks and the microstructure of 1/4 turn of the HPT-processed disks.

From **Figure 17b**, the simulation results indicate that the effective strain in the edge position varies sharply with increases in the revolutions, but the trend of the effective strain in the medium and center positions varies quite slowly. The strain distribution status leads to the microstructure results in **Figure 17c**, which the grains are obscure at the edge, and clear grains are observed in the central region. As a consequence, the hardness variation in **Figure 17a** is consistent with the trend of the effective strain, that is, the hardness varies sharply with the increasing degree of revolutions for the edge position of the HPT-processed disks but quite slowly for the medium and center positions.

In the simulation of HPT, disks occur the inhomogeneity development and distribution of strain and stress during the deformation, given the large severe plastic deformation in edge, lower deformation in center near the surface and considerable uniform deformation in radial medium of disk. The strain inhomogeneity determines the characteristic of microstructure and grains deformation even following the appearance of hardness distribution.

4.2. Effect of friction on HPT processing via finite element analysis

The HPT process involves changing the shape of the sample by forcing it to flow through a system, which requires tight contact between the die and sample. As a result of this contact, tangential frictional forces are generated at the interface of the die/sample to resist this relative movement. It is known that frictional conditions at the interface of the die/sample can affect the metal flow, finial properties of the sample, total deformation load, and premature die wear. The effect of friction between the sample and the dies is complex and results in the appearance of surface shear, particularly in HPT. Thus, friction is considered to be a major variable in metal forming processes where the sample undergoes large plastic deformations [40].

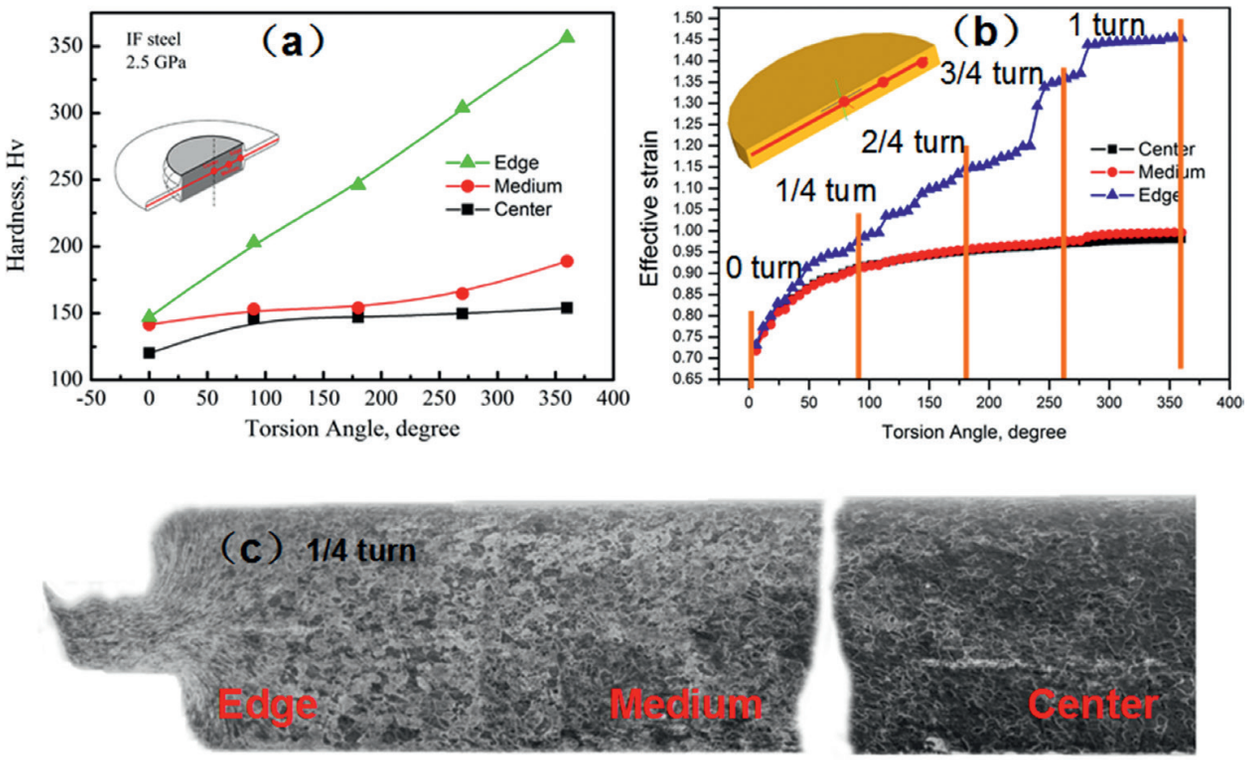

Figure 17. (a) Hardness and (b) effective strain versus rotation angle in different positions of the HPT disks, and (c) microstructure of the 1/4 turn HPT disk.

There have been preliminary investigations on the effect of friction between the anvils and workpiece on plastic deformation during the compression stage of HPT [5, 37]. The results indicated that the effective strain remarkably increased with the number of revolutions under torsion, compared to the strain in the compression stage. Although there was little variation in the central region under different friction coefficients, the strain increased significantly with distance from the center, due to frictional shear stress. Furthermore, the friction force influenced the effective strain more remarkably in the central and edge regions of the compressed disks than in the middle region. **Figure 18** shows the cross-sectional planes with effective strain distributions after compression of a copper disk under different conditions: friction coefficients of 0.1, 0.5, 1.0, and 3.0; applied pressure of 2 GPa; and wall angle of 120°.

The distribution of effective strain in the compressed copper disk is more heterogeneous as the friction coefficient increases. The radial heterogeneity of the effective strain on the plane is clearly displayed. The effective strain is lower in the center and higher at the edge of the compressed disks, and the effective strain distributions are more and more heterogeneous from center to edge. For example, with the friction coefficient of 3.0, as shown in **Figure 18d**, the variation of effective strain along the radial direction was from 0.397 in the center to 4.484 at the edge, while with friction coefficient of 0.1, the effective strain varied from 0.068 to 3.155, as shown in **Figure 18a**. This situation of heterogeneous plastic deformation was also reported in the forging process due to friction [51–55]. The results indicate that the fresh area of the contact surface, between the dies and workpiece, increased with increasing friction. Meanwhile,

http://dx.doi.org/10.5772/intechopen.68360

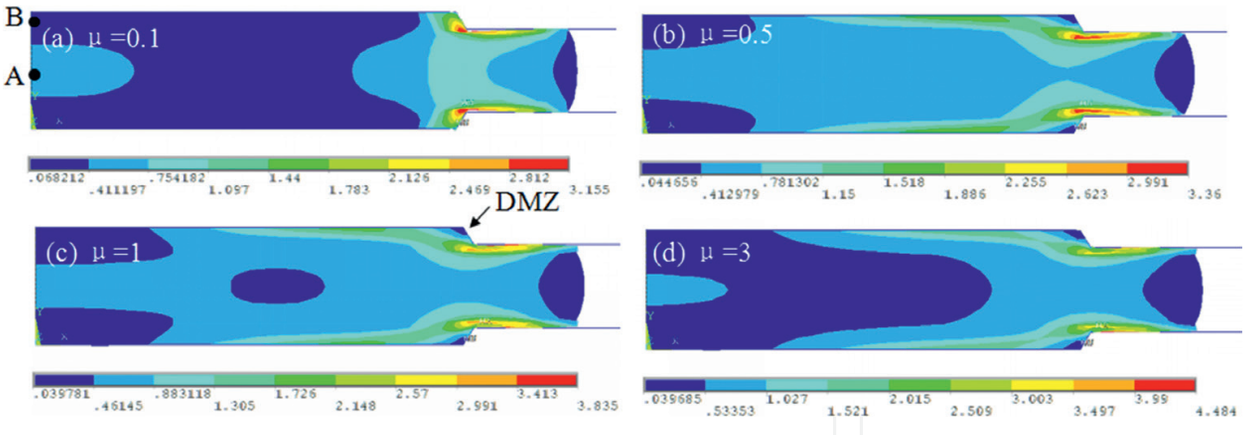

Figure 18. Effective strain distributions of the half cross-sectional planes at four friction coefficients of (a) 0.1, (b) 0.5, (c) 1.0, and (d) 3.0 under 2 GPa and 120° wall angle.

the distribution of the effective strain and hardness became more and more heterogeneous as the friction coefficient increased along the radial and axial directions, which is in good agreement with our results.

More attention should be paid to the strain distribution in the central plane of the thickness direction. The results exhibit a remarkable difference between the top and bottom planes in that the effective strain values at the center are higher than those in other areas (i.e., in the direction indicated by an arrow in **Figure 18a**. Here, an effective strain of 0.574occurred in position A (central plane), while at position B, near the surface of the upper plane, the effective strain was 0.112. Correspondingly, the hardness values of the two positions were 103.1 HV at A and 80.5 HV at B. It should be noted that the mechanical properties of the deformed material are attributable to the amount of plastic deformation (i.e., the developments and distributions of strain and stress in the workpiece during the compression process).

The hardness distribution of the experimentally compressed disks was reflected in the strain distribution of the simulations. **Figure 19** indicates the trend in variation, along the radial direction. **Figure 19** also provides a comparison between experimental hardness based on the average of four groups of experimental data, and simulation results of the effective strain distribution in the compressed copper disk, under the conditions ofa friction coefficient of 0.1, applied pressure of 2 GPa, and wall angle of 120°. The same distribution trend was indicated in both the experimental and simulated results. Hence, the reliability of this computer simulation is verified.

Figure 20 shows the evolution in effective strain at the selected point in the middle of the HPT sample for the friction coefficients of 0.5, 0.9, 1.0, and 1.5. The pressure was fixed at 10 GPa, and the number of turns was 1. Several important conclusions can be drawn from inspection of **Figure 20**. First, the effective strain values are almost the same in the compression stage at a constant of 0.4–0.6, which means that the friction had similar effect on the evolution of the effective stain on the contact surface of the HPT samples. By contrast, the effective strain is expected to increase due to the increase of the friction coefficient between the samples and the dies in the torsion stage. That is to say, the friction plays more important role on the evolution of the effective strain in the torsion stage.

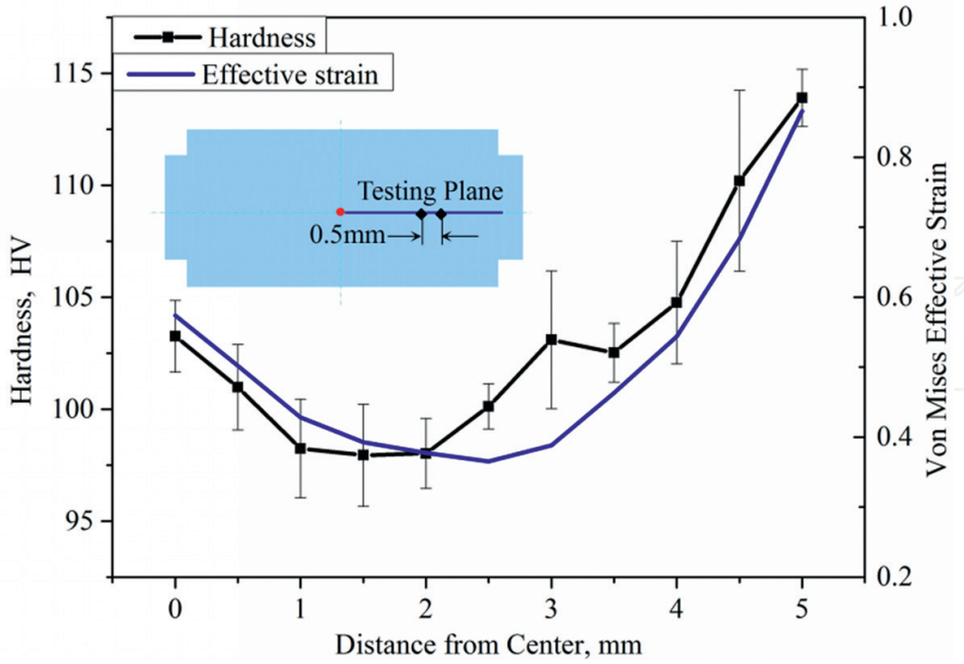

Figure 19. Path plots of the effective strain and hardness along the radial direction under 2 GPa, 120° wall angle and the friction coefficient 0.1.

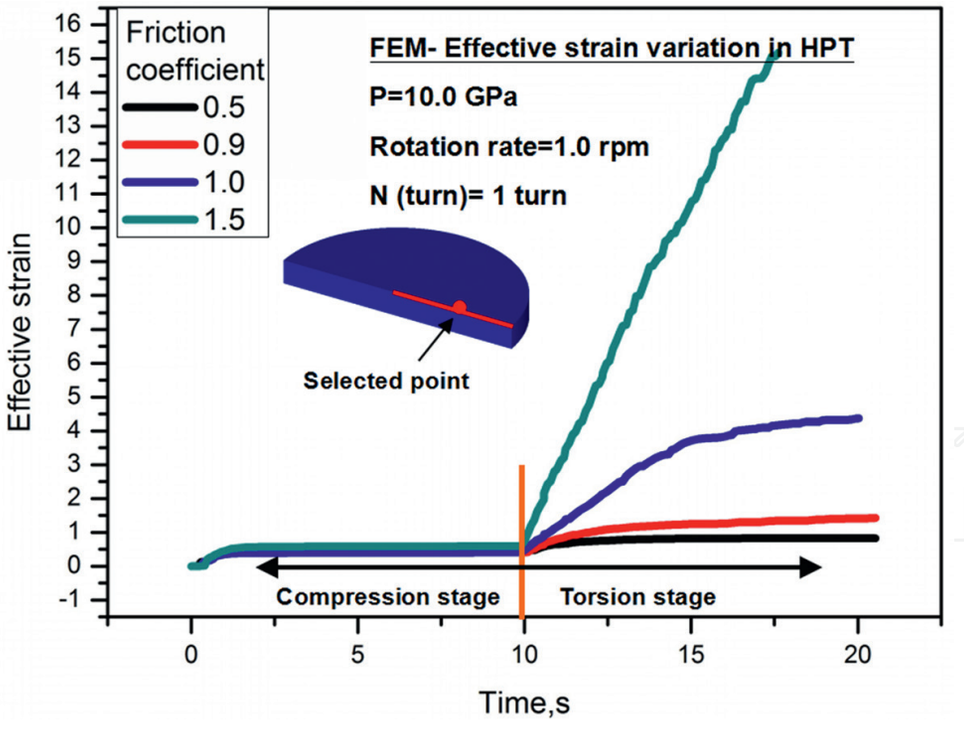

Figure 20. Simulated evolution in strain with the variation of the friction coefficient at the selected point in the medium of the HPT samples.

Another important factor is that the effective strain will reach quasi-saturation with the saturated effective strain values of 0.82, 1.33, and 4.17 when the friction coefficients are 0.5, 0.9, and 1.0, respectively. Meanwhile, the times of reaching strain saturation are also different with the

http://dx.doi.org/10.5772/intechopen.68360

variation of the friction coefficient, which are 12.1, 13.4, and 19.0 s, when the friction coefficients are 0.5, 0.9, and 1.0, respectively. Since the friction drives the surface of the sample to rotate, the effective strain remarkably increases with an increasing number of the revolutions in the torsion stage compared to strains in the compression stage. These results suggest that the friction between the sample and the dies directly affects the planes of principal stress and therefore is a major factor in the HPT process, in which the samples undergo large plastic deformation.

The simulations were performed for the friction coefficients of 0.5, 0.7, 0.9, 1.0, 1.5, and 2.0 to investigate the strain distribution on the contact surface of the HPT samples with different friction coefficients, as shown in **Figure 21a**.

Although the effective strain values in the central region were similar under different friction coefficients, the variations of effective strain according to the distance from the center had different under low (<0.9) and high (>1.0) friction coefficients. The effective strain values changed little along the distance from the center when the friction coefficients were 0.5, 0.7, and 0.9. However, the strain values increased significantly with an increasing distance from the center when the friction coefficients were 1, 1.5, and 2. The friction force affected the effective strain more in middle and edge regions than in the central region. In the middle and the edge regions, the friction shear stress due to the higher friction coefficient was high enough to achieve a sticking condition between the surfaces of the dies and the samples. **Figure 21** clearly indicates lower values of the effective strain in the central region and high values in the edge region, particularly at higher friction coefficients.

The variation of effective strain in the different position of workpiece with increasing friction coefficient is further investigated as shown in **Figure 21b**. It clearly indicates that there exist two key points of increasing friction coefficient as 0.9 and 1.5. Under the scope of friction coefficient (from 0.9 to 1.5), the effective strain sharply increases, particularly in the middle and edge area. However, it is constant variation beyond the scope (<0.9 or >1.5). That is to say, there is a friction coefficient value range which the effective strain increases remarkable sharply.

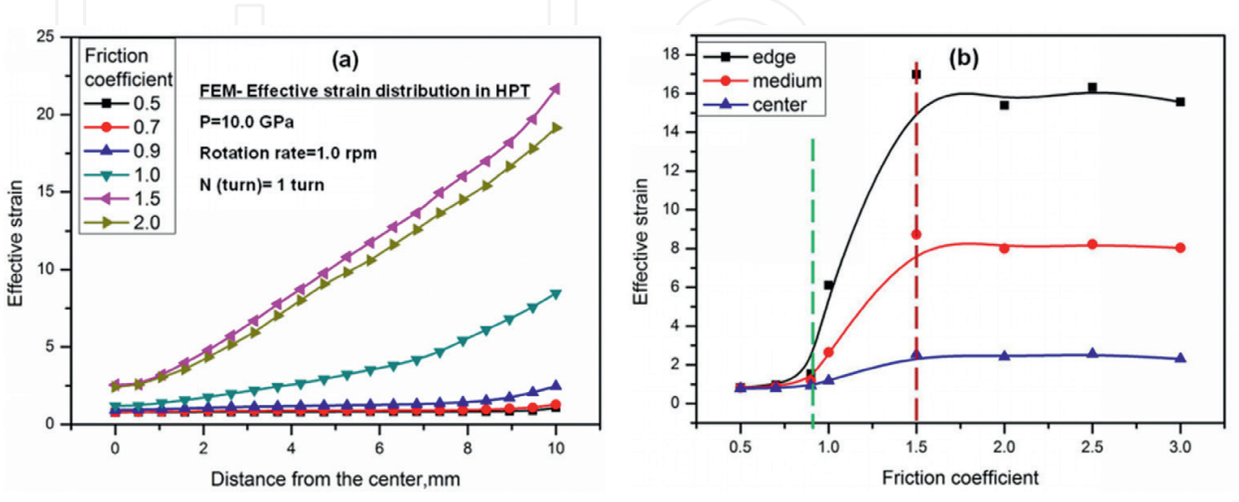

Figure 21. Simulated effective strain distribution on the contact surface of the HPT samples along with the different friction coefficient.

Compared to the compression stage, friction played an important role in the evolution of the effective strain in the torsion stage and the friction force influenced the effective strain more in the middle and edge regions than that in the central region. A high friction coefficient was enough to achieve a sticking condition between the surface of the die and the sample in medium and edge regions. Meanwhile, there is a friction coefficient value range which the effective strain increases remarkable sharply. The analysis by the finite element method for the HPT process is useful if the material parameters are incorporated. Further local and nonlocal investigations are necessary.

4.3. Effect of friction and anvil cavity structure on the dead metal zone of compressed HPT disks

The dead metal zone (DMZ) on the disks, distinct evidence of inhomogenous plastic deformation characteristics in the HPT process, was first reported by Lee et al. and verified after consideration of simulation results and inspections of microstructures from the literature [56]. In the HPT process, plastic deformation increases from the center to the edge in the radial direction of the workpiece. A sticking condition is maintained between the disk and the anvils when the traction is great enough to resist a high friction force. While there is an almost negligible strain rate and strain in the corner region, under high pressure and friction, a stagnant zone is generated due to the vertical wall constraint.

In the investigation, three factors: friction coefficient (μ), depth of the cavity on an anvil (d), and wall angle of cavity (Φ) were analyzed in the compression stage of the HPT process. The anvil structure is shown in **Figure 4**.

In the present work, the simulation results also indicated that an obvious DMZ appeared with an increase in friction coefficient (as arrow direction in **Figure 18**, and the microstructure distribution of DMZ is shown in **Figure 22** with a wall angle of 120°. There is almost no DMZ when the friction coefficient is low ($\mu = 0.1$; as shown in **Figure 18a**). Therefore, it is clear that friction remarkably influences initiation of the DMZ during the plastic deformation process in the compression stage. That is, a DMZ occurs at the corner edge of the disk under a high friction coefficient, not only in the torsion stage, but also in the compression stage of the HPT process.

Another important factor that influences initiation of the DMZ is the geometry of the anvil cavity, especially the depth of the cavity on the anvil. **Figure 23** displays the effective strain distributions on the cross-sectional planes of the compressed disks at different depths of the cavity, under conditions of 2 GPa and a friction coefficient of 0.6.

According to the effective strain distribution of the compressed disk, the degree of heterogeneity and the value of the effective strain increase as the depth of the cavity increases, along the thickness direction. **Figure 24** shows lower values of effective strain in the centers and higher values at the edges of the samples. In addition, the length of flash and the area of DMZ increase with the depth of the cavity.

Three lines of the compressed disk (**Figure 24**) were investigated in relation to DMZ, and the lines L1-L3 were effective-strain path-plot lines equally spaced from each other. The results indicated that the DMZ occurred at the surface corner of the disk and that the compressed

http://dx.doi.org/10.5772/intechopen.68360

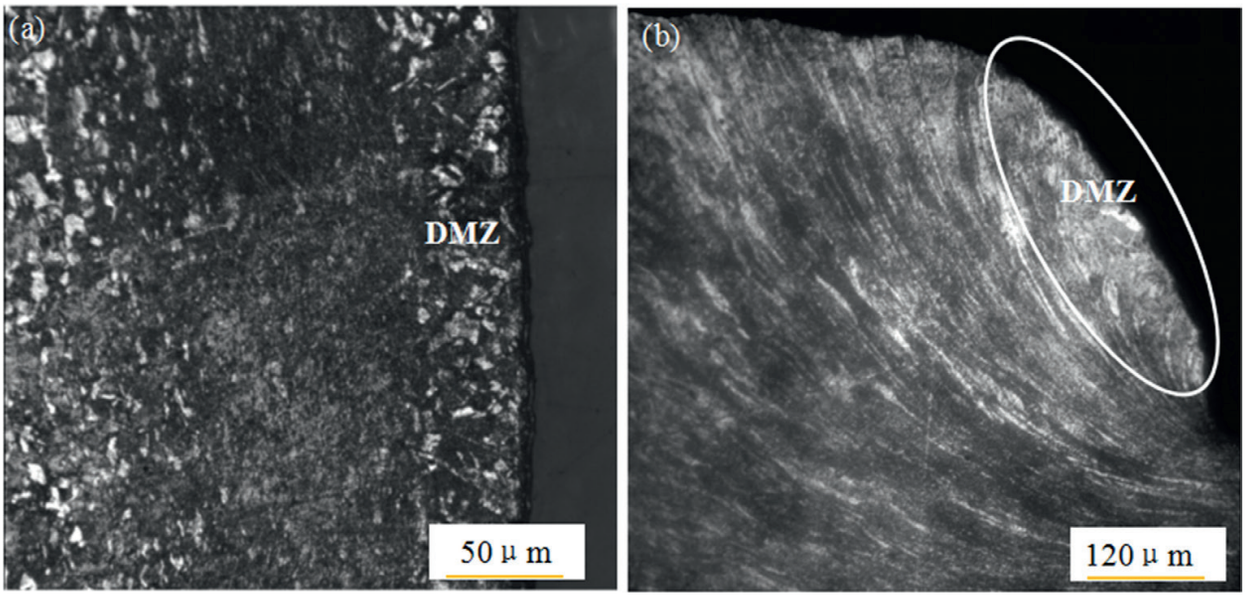

Figure 22. The microstructure distribution of DMZ on the radial direction (a) and thickness direction (b) of compressed copper disk.

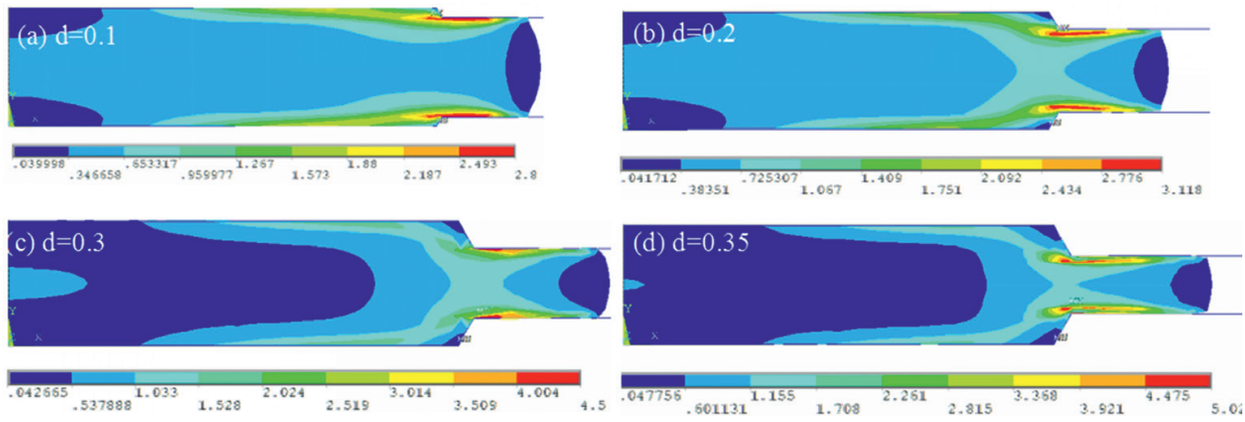

Figure 23. Effective strain distributions of the half cross-sectional planes at different depths of the cavity.

disk becomes more heterogeneous from the surface to the central plane. However, the degree of deformation in the surface region of the disk decreased with increasing depth of the cavity.

Figure 25 shows the effective strain distributions of the half cross-sectional planes along the thickness direction of a compressed copper disk, under the conditions of friction coefficient 0.1, depth 0.2 mm, and applied pressure of 2 GPa without revolution. The results can be described based on two types of HPT, unconstrained (Φ = 180°) and constrained (Φ<180°) HPT. The plastic deformation in the HPT process increased from the surface plane to the central plane of the disk. The hardness of the central plane was also higher, while the high hardness in the thick central plane as shown in **Figure 25** is called a hardness hill in the literature [32, 39]. The results indicate a variation in the hardness hill as the wall angle of the cavity is increased. However, there was almost no hardness hill at a low angle (Φ = 90°) as shown in **Figure 25a**. That is, the wall angle of the cavity can remarkably influence the hardness hill during the plastic deformation process of the compression stage.

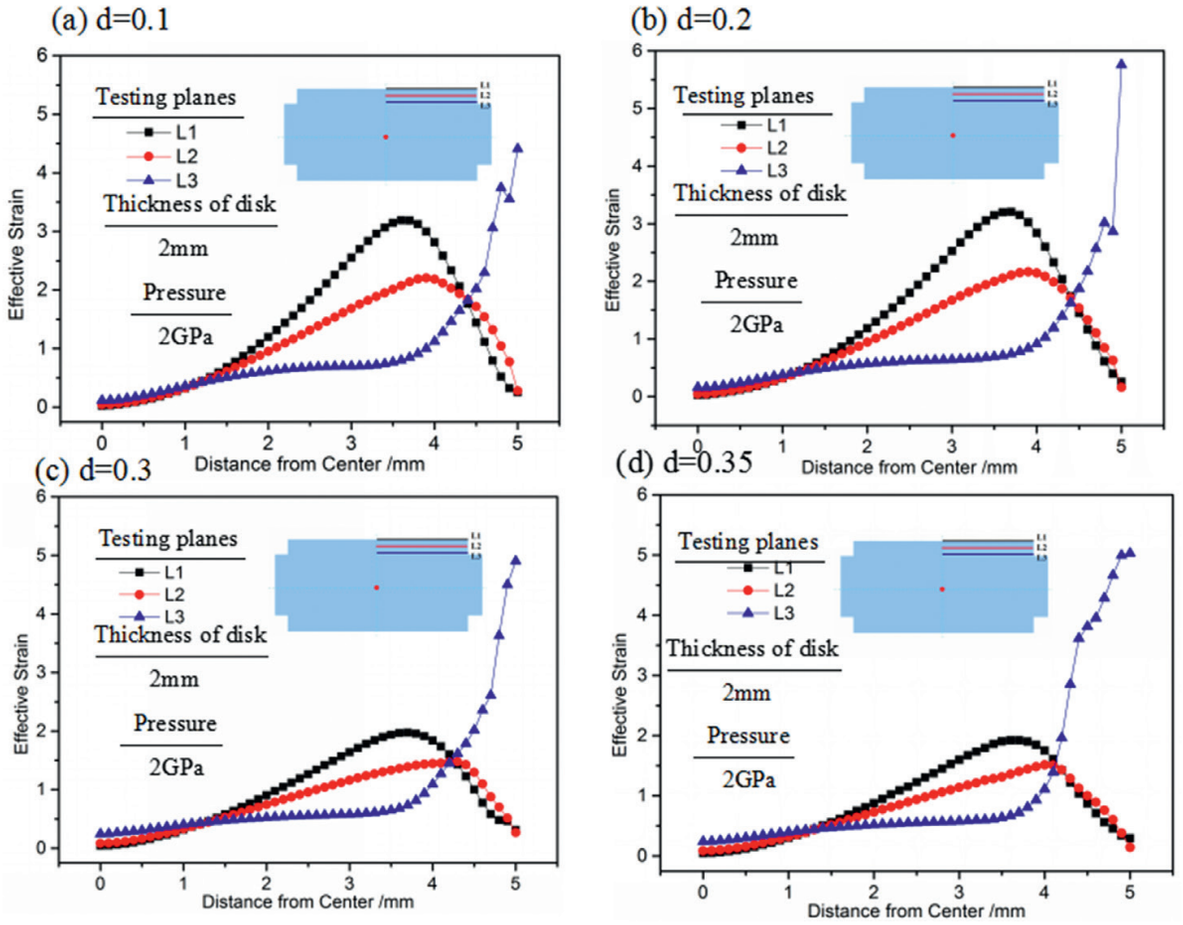

Figure 24. Path plots of the effective strain on the three lines in the disk at different depths of the cavity.

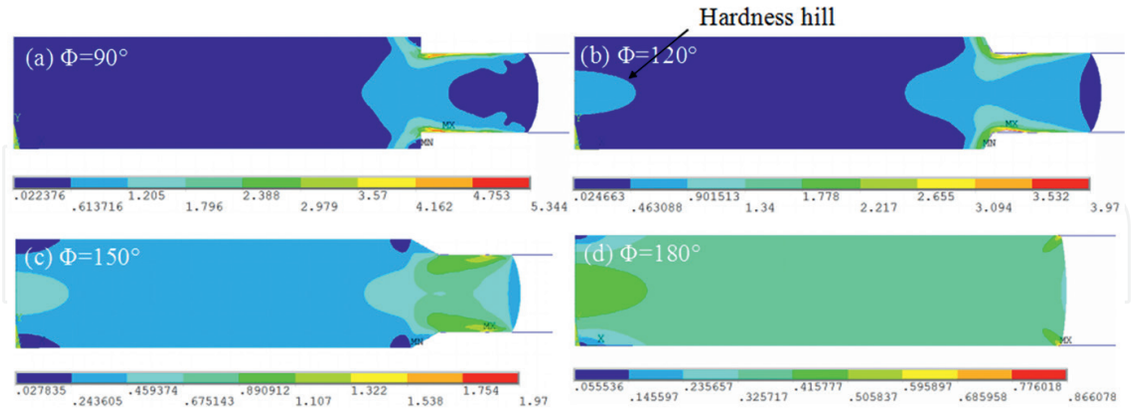

Figure 25. Effective strain distributions of the half cross-sectional planes at four wall angles of (a) 90°, (b) 120°, (c) 150°, and (d) 180° under 2 GPa and the friction coefficient 0.1.

In addition, the area of the DMZ decreased with increasing wall angle due to the vertical wall constraint under high pressure, as clearly seen in **Figure 25**, and it dropped to zero when the value of the wall angle increased to 180°, which means there is no DMZ on the disk in the unconstrained HPT processing. There was only a small variation in effective

http://dx.doi.org/10.5772/intechopen.68360

strain, and the hardness was generally homogeneous in the radial middle zones of the disks; however, a large variation occurred at the edge of the disk. Two lines were compared to determine the distribution of effective strain and are presented in **Figure 26**.

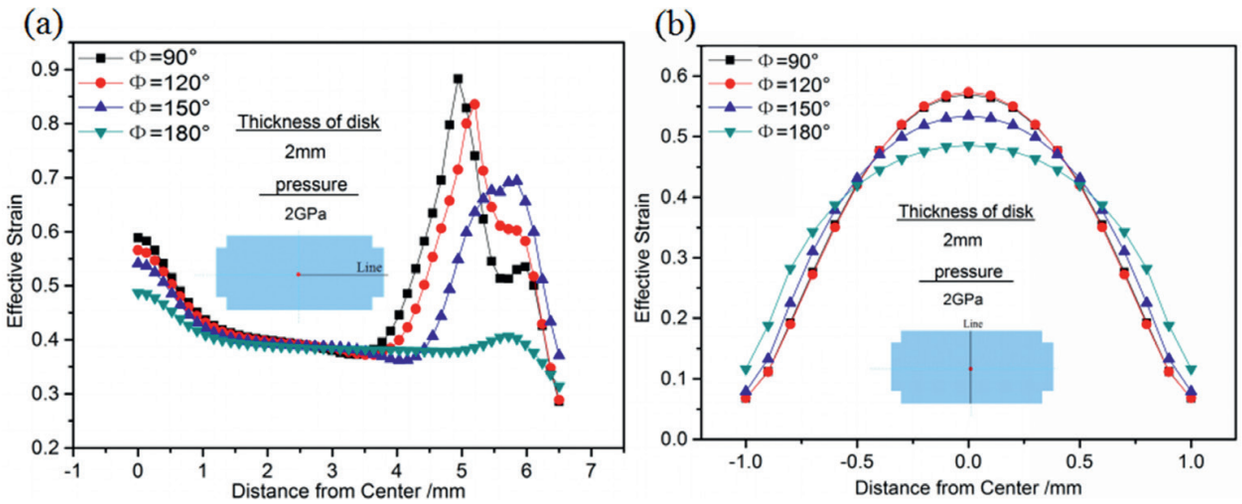

Figure 26. Path plots of the effective strain on lines listed in the disk at four wall angles of the cavity.

Figure 26 indicates that the plastic deformation was inhomogeneous along the thickness direction of the disk. Although the area of the hardness hill increased as the wall angle increased, the maximum effective strain in the area of the hardness hill decreased as the angle increased, as shown in **Figure 26b**. There was significant plastic deformation when the wall angle was less than 180° (indicated in **Figure 26a**), while the plastic deformation was relatively uniform along the radial direction under the wall angle condition of 180°. In addition, the anvil geometry also affected the flash of the disk. Interestingly, there was little variation in the flash length of the compressed disk at different wall angles, although a large distinction of strain in the flash regions happened. In any case, the wall angle of the cavity plays an important role in the heterogeneous deformation of the main body of the workpiece.

5. Effect of Hollowcone high-pressure torsion on the thermal and mechanics properties of Zr-based bulk metallic glass

Bulk metallic glasses (BMGs) usually have many outstanding properties, for example, good corrosion resistance [57], high elastic limits [58], high strength [59], and so on. However, the limited plastic deformability at room temperature is a problem awaiting solution, which seriously hindered the application of BMGs. However, BMGs under the condition of HPT exhibit a certain plasticity deformability at room temperature. The results from literatures indicated that the hardness of HPT BMGs disks decreased due to the rejuvenated structure, which is completely different phenomenon in the crystalline alloys. There also have some research reported that effects on the thermal properties of BMGs happened. For example, Edalati et al. reported that

the glass transition temperature of $Zr_{50}Cu_{30}Ni_{10}Al_{10}$ BMG increased few after a HPT process [60]. However, Meng et al. reported that HPT did not change the glass transition temperature [61].

In particular, Kim et al. proposed that a hollow cone high-pressure torsion (HC-HPT) method used for the fabrication of hollow cone-shaped specimens with a closed cone head through the application of high pressure and torsion in order to obtain UFG/NC microstructures [62]. Therefore, it is an interesting and necessary attempt to research the effects of hollow cone high-pressure torsion on the performance of BMGs.

In this section, $Zr_{64.13}Cu_{15.75}Ni_{10.12}Al_{10}$ BMGs [63] were selected as a specimen material to research the effect of hollow-cone high-pressure torsion on the performance of BMGs. Because Zr-based BMGs have satisfactory glass-forming abilities, it can be undemanding cast into a hollow cone-shaped specimen. Furthermore, the catastrophic failure at room temperature will not occur by the HC-HPT process due to superior plastic deformability at room temperature.

Hóbora et al. reported that $Cu_{60}Zr_{20}Ti_{20}$ BMGs occurred crystallization after HPT process [64]. On the contrary, some research data indicate that BMGs did not occurred crystallization after HPT process. Therefore, first make sure whether the sample occurred crystallization after HC-HPT process. **Figure 27** shows the X-ray diffraction (XRD) patterns for the transverse cross sections of as-cast and HC-HPT 1 revolution BMG alloys.

The XRD patterns have similar profiles. The broad diffraction peaks indicate full vitrification of samples, and crystalline peaks were not detected. This indicates that no crystallization did occur in the $Zr_{64.13}Cu_{15.75}Ni_{10.12}Al_{10}$ BMG through HC-HPT 1 revolution. The plastic deformation during the HC-HPT process was reduced, conical wall thickness slight due to the sample has been reversed only one revolution.

HPT process changes the microstructure of the BMGs, even though have not induced crystallization, and inevitably have a certain effect on its thermodynamic properties. **Figure 28** presents the DSC profiles for the as-cast and HC-HPT 1 revolution samples.

The curves have similar profiles. They have well-defined glass transition regions. However, the characteristic temperatures of glass transition and crystallization are different. The Figure shows that the glass transition begins at 657.63 K and ends at 736.23 K for the as-cast sample, and it begins at 663.19 K and ends at 759.19 K for the HC-HPT 1 revolution sample. It is found that, after HC-HPT, supercooled liquid region increases.

The effects of HC-HPT process on the glass transition and crystallization behaviors for the Zr-based BMG are remarkable. The results happened by the increase of free volume after the large shear deformation of HC-HPT. The increase of free volume usually leads to a decrease in hardness and elastic modulus.

Figure 29 presents the curves of thermal expansion for the as-cast and HC-HPT 1 revolution processed at a heating rate of 0.0833 K/s. These curves exhibit similar thermal expansion behaviors. From the room temperature to around 640 K, the length of the both samples increased linearly to a temperature. Then, the lengths have decreased which suggest related to the crystallization of the alloys. Obviously, the average thermal expansion coefficient has

http://dx.doi.org/10.5772/intechopen.68360

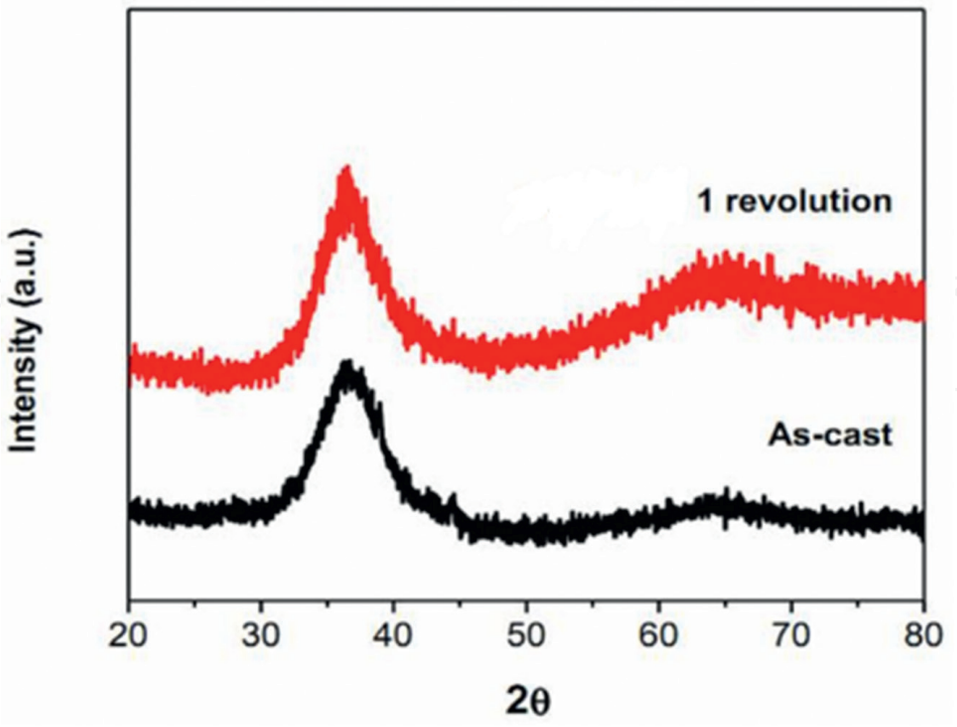

Figure 27. The XRD pattern of samples before and after deformation.

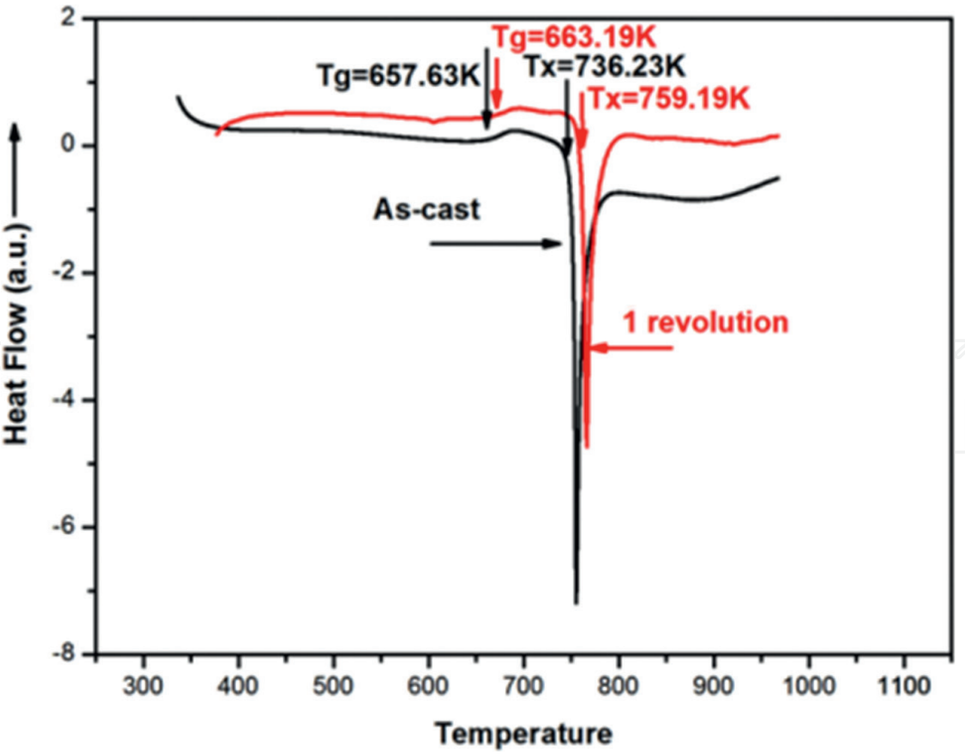

Figure 28. The DSC pattern of samples before and after deformation.

decreased after the HC-HPT process. The free volume can be created by the inelastic deformation of local atomic clusters under shear stress [65]. After the HC-HPT process, the free volume in the sample increased. Therefore, the sample was heated, and the created free volume by HC-HPT processed disappears due to a decrease in the thermal expansion coefficient.

Tan et al. [66] reported that the plasticity deformation corresponds to the internal states with more free volume as revealed by lower hardness and elastic modulus. **Figure 30** presents the hardness curve from cone vertical top to bottom.

The two patterns have similar profile, and the hardness of sample cone is tending to descend from top to bottom of the hollow cone. Compared with the sample before deformation, the hardness has decreased after HC-HPT. The results were coinciding with the increase of free volume. The same results were obtained for the elastic modulus test as shown in **Table 2**.

Table 2 presents the results using nano indentation method of elastic modulus of specimen at different position. And compared with HC-HPT 1 revolution sample, HC-HPT deformation makes the elastic modulus of amorphous alloy reduces. Different parts have different elastic modulus with a sample due to the special sample shape give rise to different cooling rates. A larger amount of free volume around atoms may enlarge their internal atomic spacing, decrease the atomic bonding strength, and thus lower the elastic modulus of the amorphous alloy [67].

In this study, hollow cone Zr-based amorphous has been chosen to be the investigated. Severe plastic deformation using HC-HPT with one revolution has effects on the thermal and mechanical properties of $Zr_{64.13}Cu_{15.75}Ni_{10.12}Al_{10}$ BMGs. It was found that after the HC-HPT process, the glass transition temperature of Zr-based BMG increased, but the Vickers hardness, elastic modulus, and coefficient of thermal expansion decreased.

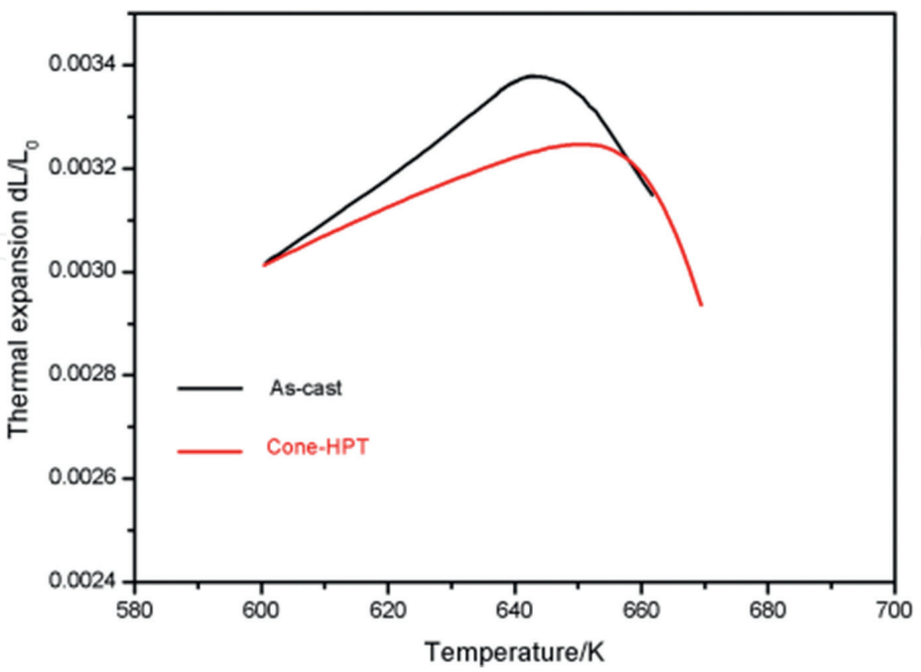

Figure 29. Dilatometer traces of the as-cast and cone-HPT processed.

http://dx.doi.org/10.5772/intechopen.68360

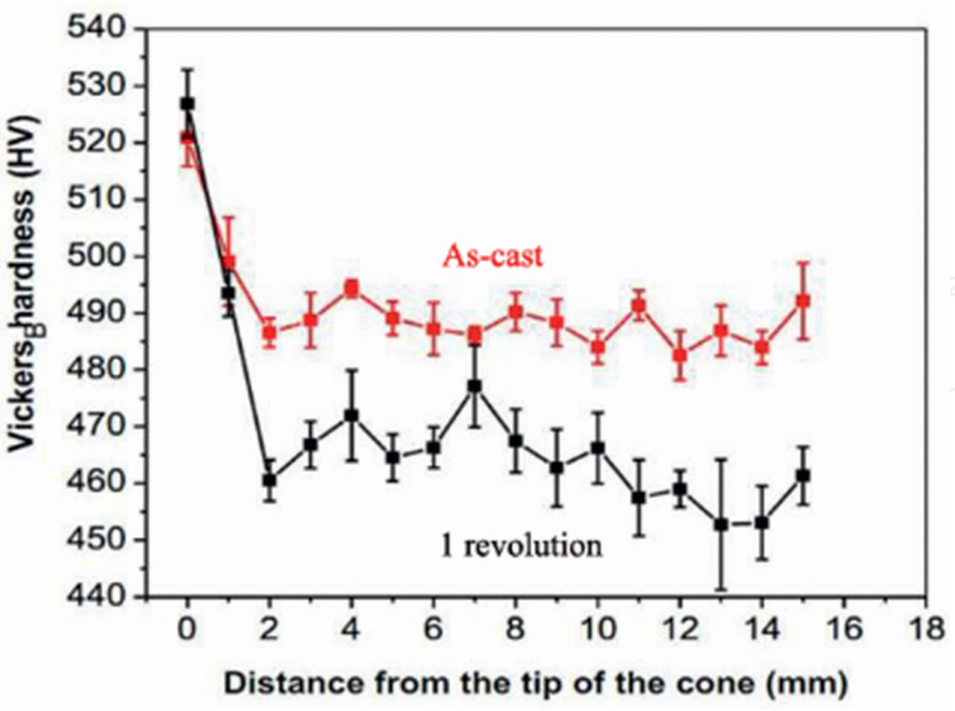

Figure 30. Vickers hardness of samples at different locations before and after HC-HPT.

Samples	E of top part (GPa)	E of middle part (GPa)	E of bottom part (GPa)
As-cast	95.16	92.92	82.43
One revolution	93.76	89.67	76.23

Table 2. Elastie modulus of specimens at different locations before and after HC-HPT.

Author details

Yuepeng Song[1]*, Wenke Wang[1,2], Miaomiao Chen[1], Jing Guo[1], Lingfeng Xu[1], Dongsheng Gao[1] and Hyoung Seop Kim[3]

*Address all correspondence to: ustbsong@sina.com

1 Shandong Provincial Key Laboratory of Horticultural Machineries and Equipments, Mechanical and Electronic Engineering College, Shandong Agricultural University, Tai'an, PR China

2 School of Materials Science and Engineering, Harbin Institute of Technology, Weihai, PR China

3 Department of Materials Science and Engineering, Pohang University of Science and Technology, Pohang, Korea

References

[1] Xie ZL, Xie JJ, Hong YS, Wu XL. Influence of processing temperature on microstructure and microhardness of copper subjected to high-pressure torsion. Science China Technological Sciences. 2010;**53**:1534-1539

[2] Kim HS, Estrin Y, Bush MB. Plastic deformation behaviour of fine-grained materials. Acta Materialia. 2000;**48**(2):493-504

[3] Kim HS, Estrin Y. Ductility of ultrafine grained copper. Applied Physics Letters. 2001; **79**:4115-4117

[4] Xu Ch, Horita ZJ, Langdon TG. The evolution of homogeneity in an aluminum alloy processed using high-pressure torsion. Acta Materialia. 2008;**56**:5168-5176

[5] Zhilyaev AP, Langdon TG. Using high-pressure torsion for metal processing: Fundamentals and applications. Progress in Materials Science. 2008;**53**:893-895

[6] Moon S, Kim JH, Shim JY, Ahn YB, Song KH. Analysis of aberrantly spliced HRPT2 transcripts and the resulting proteins in HPT-JT syndrome. Molecular Genetics and Metabolism. 2010;**100**:365-371

[7] Zhilyaev AP, Gimazov AA, Soshnikova EP, Révész Á, Langdon TG. Microstructural characteristics of nickel processed to ultrahigh strains by high-pressure torsion. Materials Science and Engineering A. 2008;**489**:207-212

[8] Zhilyaev AP, Oh-ishi K, Langdon TG, McNelley TR. Microstructural evolution in commercial purity aluminum during high-pressure torsion. Materials Science and Engineering A. 2005;**410-411**:277-280

[9] Lugo N, Llorca N, Cabrera JM, Horita Z. Microstructures and mechanical properties of pure copper deformed severely by equal-channel angular pressing and high pressure torsion. Materials Science and Engineering A. 2008;**477**:366-371

[10] Kurmanaeva L, Ivanisenko Y, Markmann J, Kübel C, Chuvilin A, Doyle S, Valiev RZ, Fecht HJ. Grain refinement and mechanical properties in ultrafine grained Pd and Pd–Ag alloys produced by HPT. Materials Science and Engineering A. 2010;**527**:1776-1783

[11] Kawasaki M, Ahn B, Langdon TG. Effect of strain reversals on the processing of high-purity aluminum by high-pressure torsion. Journal of Materials Science. 2010 (online)

[12] Zhilyaev AP, McNelley TR, Langdon TG. Evolution of microstructure and microtexture in fcc metals during high-pressure torsion. Journal of Materials Science. 2007;**42**:1517-1528

[13] Valiev RZ, Islamgaliev RK, Alexandrov IV. Bulk nanostructured materials from severe plastic deformation. Progress in Materials Science. 2000;**45**:103-189

[14] Yoo SJ, Kim WJ. Microstructure and strengthening mechanisms of carbon nanotube reinforced magnesium matrix composites fabricated by accumulative roll bonding. Korean Journal of Metals and Materials. 2014;**52**:561-172

[15] Valiev RZ, Langdon TG. Principles of equal-channel angular pressing as a processing tool for grain refinement. Progress in Materials Science. 2006;**51**:881-981

[16] Lee SH, Saito Y, Tsuji N, Utsunomiya H, Sakai T. Role of shear strain in ultragrain refinement by accumulative roll-bonding (ARB) process. Scripta Materialia. 2002;**46**:281-285

[17] Takayama Y, Sasaki J, Kato H, Watanabe H. Improvement of fatigue properties by means of continuous cyclic bending and annealing in an Al-Mg-Mn alloy sheet. Materials Transactions. 2004;**45**:1833-1838

[18] Dong HS, Kim I, Kim J, Zhu YT. Shear strain accommodation during severe plastic deformation of titanium using equal channel angular pressing. Materials Science and Engineering A. 2002;**334**:239-245

[19] Pourrahimi S, Nayeb Hashemi H, Foner S. High-strength high-conductivity Cu-Nb microcomposite wire by powder metallurgy. Journal of Materials Science Letters. 1990; **9**:1484-1487

[20] Prangnell PB, Harris C, Roberts SM. Finite element modeling of equal channel angular extrusion. Scripta Materialia. 1997;**37**:983-989

[21] Chang SY, Lee JG, Park KT, Dong HS. Microstructures and mechanical properties of equal channel angular pressed 5083 Al alloy. Materials Transactions. 2001;**42**:1074-1080

[22] Nakamura K, Neishi K, Kaneko K, Nakagaki M, Horita Z. Development of severe torsion straining process for rapid continuous grain refinement. Materials Transactions. 2004;**45**:3338-3342

[23] Orlov D, Beygelzimer Y, Synkov S, Varyukhin V, Tsuji N, Horita Z. Microstructure evolution in pure Al processed with twist extrusion. Materials Transactions. 2009;**50**:96-100

[24] Bridgman PW. Effects of high shearing stress combined with high hydrostatic pressure. APS Journals Archive. 1935;**48**:825-847

[25] Valiev RZ, Krasilnikov NA, Tsenev NK. Plastic deformation of alloys with submicron-grained structure. Materials Science and Engineering:A. 1991;**137**:35-40

[26] Figueiredo RB, Aguilar MT, Cetlin PR, Langdon TG. Deformation heterogeneity on the cross-sectional planes of a magnesium alloy processed by high-pressure torsion. Metallurgical and Materials Transactions A. 2011;**42**:3013-3021

[27] Hohenwarter A, Bachmaier A, Gludovatz B, Scheriau S, Pippan R. Technical parameters affecting grain refinement by high pressure torsion. International Journal of Materials Research. 2009;**100**:1653-1661

[28] Kim HS, Joo SH, Jeong HJ. Plastic deformation and computer simulations of equal channel angular pressing. Korean Journal of Metals and Materials. 2014;**52**:87-99

[29] Kim HS, Ryu WS, Janecek M, Baik SC, Estrin Y. Effect of equal channel angular pressing on microstructure and mechanical properties of IF steel. Advanced Engineering Materials. 2005;**7**:43-45

[30] Bridgman PW. On torsion combined with compression. Journal of Applied Physics. 1943;**14**:273-281

[31] Sakai G, Nakamura K, Horita Z, Langdon TG. Developing high-pressure torsion for use with bulk samples. Materials Science and Engineering A. 2005;**406**:268-273

[32] Song YP, Wang WK, Lee DJ, Jeong HJ, Lee S, Kim HS. Thickness inhomogeneity in hardness and microstructure of copper after the compressive stage in high-pressure torsion. Metals and Materials International. 2015;**21**:7-13

[33] Xu Ch, Horita ZJ, Langdon TG. Microstructural evolution in pure aluminum in the early stages of processing by high-pressure torsion. Materials Transaction. 2010;**51**:2-7

[34] Xu Ch, Horita ZJ, Langdon TG. The evolution of homogeneity in processing by high-pressure torsion. Acta Materialia. 2007;**55**:203-212

[35] Hadzima B, Janecek M, Estrin Y, Hyoung SK. Microstructure and corrosion properties of ultrafine-grained interstitial free steel. Materials Science and Engineering A. 2007;**462**:243-247

[36] Song YP, Wang WK, Gao DS, Kim HS, Yoon EY, Lee DJ, Lee CS, Guo J. Inhomogeneous hardness distribution of high pressure torsion processed IF steel disks. Materials Sciences and Applications. 2012;**3**:234-239

[37] Song YP, Wang WK, Gao DS, Yoon EY, Lee DJ, Kim HS. Finite element analysis of the effect of friction in high pressure torsion. Metals and Materials International. 2014;**20**:445-450

[38] Wang WK, Song YP, Yoon EY, Lee DJ, Lee JH, Kim HS. Analysis of stress states in the compression stage of high pressure torsion using the slab analysis method and the finite element method. Metals and Materials International. 2013;**5**:1021-1027

[39] Song YP, Wang WK, Gao DS, Yoon EY, Lee DJ, Lee CS, Kim HS. Hardness and microstructure of interstitial free steels in the early stage of the high-pressure torsion process. Journal of Materials Science. 2013;**48**:4698-4704

[40] Song YP, Yoon EY, Lee DJ, Lee JH, Kim HS. Mechanical properties of copper after compression stage of high-pressure torsion. Materials Science and Engineering A. 2011;**528**:4840-4844

[41] http://www.matweb.com

[42] Edalati K, Fujioka T, Horita Z. Microstructure and mechanical properties of pure Cu processed by high-pressure torsion. Materials Science and Engineering A. 2008;**497**:168-173

[43] Wang WK, Song YP, Kim HS. Experimental and finite element analyses of plastic deformation in the compressive stage of copper in high-pressure torsion. Rare Metal Materials and Engineering. 2011;**40**:301-304

[44] Vorhauer A, Pippan R. On the homogeneity of deformation by high pressure torsion. Scripta Materialia. 2004;**51**:921-925

[45] Figueiredo RB, Langdon TG. Fabricating ultrafine-grained materials through the application of severe plastic deformation: A review of developments in Brazil. Journal of Materials Research and Technology. 2012;**1**:55-62

[46] Bachmaier A, Kerber M, Setman D, Pippan R. The formation of supersaturated solid solutions in Fe-Cu alloys deformed by high-pressure torsion. Acta Materialia. 2012;**60**:860-871

[47] Xum C, Horita Z, Langdon TG. Evaluating the influence of pressure and torsional strain on processing by high-pressure torsion. Journal of Materials Science. 2008;**43**:7286-7292

[48] Kawasaki M, Langdon TG. The significance of strain reversals during processing by high-pressure torsion. Materials Science and Engineering: A. 2008;**498**:341-348

[49] Yoon SC, Nagasekhar AV, Kim HS. Finite element analysis of the bending behavior of a workpiece in equal channel angular pressing. Metals and Materials International. 2009;**15**:215-219

[50] Ivanisenko Y, Lojkowski W, Valiev RZ, Fecht HJ. The mechanism of formation of nanostructure and dissolution of cementite in a pearlitic steel during high pressure torsion. Acta Materialia. 2003;**51**:5555-5570

[51] Horita Z, Langdon TG. Achieving exceptional superplasticity in a bulk aluminum alloy processed by high-pressure torsion. Scripta Materialia. 2008;**58**:1029-1032

[52] Shen G, Vedhanayagam A, Kropp E. A method for evaluating friction using a backward extrusion-type forging. Journal of Materials Processing Technology. 1992;**33**:109-123

[53] Narayanan RG, Gopal M, Rajadurai A. Influence of friction in simple upsetting and prediction of hardness distribution in a cold forged product. Journal of Testing and Evaluation. 2008;**36**:371-383

[54] Xu SQ, Chen ZY, Zhang SY. Research on the relation between bulging and friction in cylinder upsetting. Forging and Stamping Technology(in Chinese). 2004;**29**:46-48

[55] Lu P, Zhao GQ, Guan YJ, Cheng JL. Thickness of decarburized Layer can be calculated by Fick's Law of diffusion. China Metal Forging Equipment and Manufacturing Technology (in Chinese). 2008;**43**:75-79

[56] Lee DJ, Yoon EY, Park LJ, Kim HS. The dead metal zone in high-pressure torsion. Scripta Materialia. 2012;**67**:384-387

[57] Li YH, Zhang W, Qin FX, Makino A. Mechanical properties and corrosion resistance of a new $Zr_{56}Ni_{20}Al_{15}Nb_4Cu_5$ bulk metallic glass with a diameter up to 25mm. Journal of Alloys and Compounds. 2014;**615**:71-74

[58] Zong HT, Bian LY, Cheng JY, Cao GH, Kang CY, Li M. Glass forming ability, thermal stability and elastic properties of Zr-Ti-Cu-Be-(Fe) bulk metallic glasses. Results in Physics. 2016;**6**:1157-1160

[59] Zhou XL, Zhou HF, Li XY, Chen CQ. Size effects on tensile and compressive strengths in metallic glass nanowires. Journal of the Mechanics and Physics of Solids. 2015;**84**:130-144

[60] Edalati K, Yokoyama Y, Horita Z. High-pressure torsion of machining chipsand bulk discs of amorphous $Zr_{50}Cu_{30}Al_{10}Ni_{10}$. Materials Transactions. 2010;**51**:23-26

[61] Meng FQ, Tsuchiya SK, Yokoyama Y. Reversible transition of deformation mode by structural rejuvenation and relaxation in bulk metallic glass. Applied Physics Letter. 2012;**101**:121914

[62] Um HY, Yoon EY, Lee DJ, Lee CS, Park LJ, Lee S, Kim HS. Hollow cone high-pressure torsion: Microstructure and tensile strength by unique severe plasticdeformation. Scripta Materialia. 2014;**71**:41-44

[63] Liu YH, Wang G, Wang RJ, Zhao DQ, Pan MX, Wang WH. Super plastic bulk metallic glassesat room temperature. Science. 2007;**315**:1385-1388

[64] Hóbora S, Kovács Z, Révész Á. Estimation of heat production during high pressure torsion of Cu-based metallic glass. Journal of Alloys and Compounds. 2010;**495**:352-355

[65] Steif PS, Spaepen F, Hutchinson JW. Strain localization in amorphous metals. Acta Metallurgica. 1982;**30**:447-455

[66] Tan J, Zhang Y, Sun BA, Stoica M, Li CJ, Song KK, Kühn U, Pan FS, Eckert J. Correlation between internal states and plasticity in bulk metallic glass. Applied Physics Letters. 2011;**98**:15

[67] Li N, Liu L, Chen Q, Pan J, Chan KC. The effect of free volume on the deformation behaviour of a Zr-based metallic glass under nanoindentation. Journal of Physics D: Applied Physics. 2007;**40**:19